Chapter 2

Bonding in Solids

Crystalline materials exhibit the complete spectrum of bond types, ranging from ionic to covalent, van der Waals and metallic. Sometimes more than one type of bonding is present, as in salts of complex anions, e.g. Li_2SO_4, which have both ionic and covalent bonds. Commonly, the bonds are a blend of different types, as in TiO which is ionic/metallic or CdI_2 which is ionic/covalent/van der Waals. In discussing structures, it is often convenient to ignore temporarily the complexities of mixed bond types and to treat bonds as though they were purely ionic.

Ionic bonding leads to structures with high symmetry in which the coordination numbers are as high as possible. In this way, the net electrostatic attractive force which holds crystals together (and hence the lattice energy) is maximized. *Covalent bonding*, by contrast, gives highly directional bonds in which atoms prefer a certain coordination environment, irrespective of other atoms that are present. The coordination numbers in covalent structures are usually small and may be less than those in ionic structures which contain similar-sized atoms.

The bonding in a particular compound correlates fairly well with the position of the component atoms in the periodic table and, especially, with their electronegativity. Alkali and alkaline earth elements usually form ionic structures (Be is sometimes an exception), especially in combination with small electronegative anions such as O^{2-} and F^-. Covalent structures occur especially with: (a) small atoms of high valency which, in the cationic state, would be highly polarizing, e.g. $B^{3+}, Si^{4+}, P^{5+}, S^{6+}$, etc.; and to a lesser extent with (b) large atoms which in the anionic state are highly polarizable, e.g. I^-, S^{2-}.

Most non-molecular materials have mixed ionic and covalent bonding and, as discussed later, it is possible to assess the *ionicity* of a particular bond, i.e. the percentage of ionic character in the bond. An additional factor in some transition metal compounds especially is the occurrence of metallic bonding.

2.1 Ionic bonding

Purely ionic bonding rarely occurs. Even structures that are regarded as classically ionic, e.g. NaCl and CaO, usually have some partial covalent character. The degree of covalent bonding increases with increasing valence and ions with a *net* charge greater than +1 or −1 are unlikely to exist. Thus, while NaCl may

reasonably be represented as Na^+Cl^-, TiC (which also has the NaCl structure) certainly does not contain Ti^{4+} and C^{4-} ions and the main bonding type in TiC must be non-ionic. This brings us to a dilemma. Do we continue to use the ionic model in the knowledge that for many structures, e.g. Al_2O_3, $CdCl_2$, a large degree of covalent bonding must be present? If not, we must find an alternative model for the bonding. In this section, ionic bonding is given prominence because of its apparent wide applicability and its usefulness as a *starting point* for describing structures which in reality often have considerable covalent bonding.

2.2 Ions and ionic radii

It is difficult to imagine discussing crystal structures without having definitive information on the sizes of ions in crystals. However, crystal chemistry has undergone a minor revolution recently because the long-established tables of ionic radii of Pauling, Goldschmidt and others are now thought to be seriously

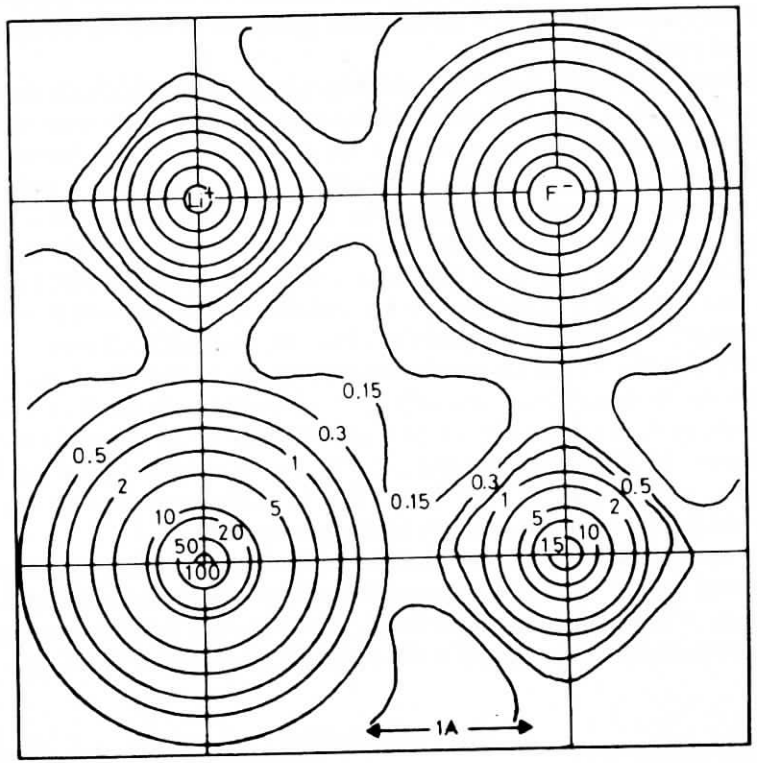

Fig. 2.1 Electron density contour map of LiF (rock salt structure): a section through part of the unit cell face. The electron density (electrons $Å^{-3}$) is constant along each of the contour lines. (From Krug, Witte and Wolfel, *Zeit. Phys. Chem., Frankfurt*, **4**, 36, 1955)

in error; at the same time, our concepts of ions and ionic structures have undergone revision. In more recent compilations of ionic radii, e.g. of Shannon and Prewitt (1969, 1970), cations are larger and anions smaller than previously thought. For example, Pauling radii of Na^+ and F^- are 0.98 and 1.36 Å, respectively, whereas Shannon and Prewitt give values of 1.14 to 1.30 Å, depending on the coordination number, for Na^+, and 1.19 Å for F^-.

These changes have arisen because, high-quality X-ray diffraction work gives fairly accurate maps of the distribution of electron density throughout crystals. Thus, one can effectively 'see' ions and tell something about their size, shape and nature. Fig. 2.1 shows an electron density 'contour map' of LiF for a section passing through the structure parallel to one unit cell face. The map therefore passes through the centres of Li^+ and F^- ions located on the (100) planes. Fig. 2.2 shows the variation of electron density with distance along the line that connects adjacent Li^+ and F^- ions. From Figs 2.1 and 2.2 and similar diagrams for other structures, the following conclusions about ions in crystals may be drawn:

(a) Ions are essentially spherical.
(b) Ions may be regarded as composed of two parts: a central core in which most of the electron density is concentrated and an outer sphere of influence which contains very little electron density.
(c) Assignment of radii to ions is difficult; even for ions which are supposedly in contact, it is not obvious (Fig. 2.2) where one ion ends and another begins.

Conclusion (b) is in contrast to the oft-stated assumption that 'ions can be treated as charged, incompressible, non-polarizable spheres'. Certainly, ions are charged, but they cannot be regarded as hard spheres with a clearly defined

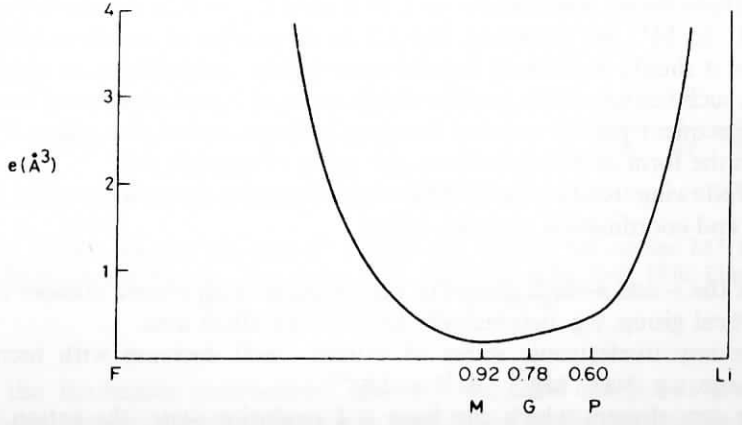

Fig. 2.2 Variation of electron density along the line connecting adjacent Li and F nuclei in LiF. (From Krebs, *Fundamentals of Inorganic Crystal Chemistry*, 1968.) P = Pauling radius of Li^+, G = Goldschmidt radius, M = minimum in electron density

radius. Their electron density does not decrease abruptly to zero at a certain distance from the nucleus but instead decreases roughly exponentially with increasing radius. Instead of being incompressible, ions are quite elastic, by virtue of flexibility in the outer sphere of influence of an ion while the inner core remains unchanged. This flexibility is necessary in order to explain variations of apparent ionic radii with coordination number and environment (see later). Within limits, ions can expand or contract as the situation demands.

From Figs 2.1 and 2.2, most electron density is concentrated close to the nuclei of ions; in a crystal, therefore, most of the total volume is essentially free space and contains relatively little electron density. It is not completely ludicrous to draw an analogy between the structure of an atom (or ion) and that of our solar system. In both, most of the matter is concentrated in relatively small regions and the rest of the volume is made up of essentially empty space.

It is difficult to determine ionic radii because, between adjacent anions and cations, the electron density passes through a broad, shallow minimum. For LiF, Fig. 2.2, the radii for Li^+ given by Pauling and Goldschmidt are marked together with the value corresponding to the minimum in the electron density along the line connecting Li^+ and F^-. Although the values of these radii vary from 0.60 to 0.92 Å, all lie within the broad electron density minimum of Fig. 2.2.

In spite of the difficulties in determining absolute radii, it is necessary to have a set of radii for reference. Fortunately, most sets of radii are *additive* and *self-consistent*; provided one does not mix radii from different tabulations it is possible to use any set of radii to evaluate interionic distances in crystals with reasonable confidence. Shannon and Prewitt give two sets of radii: one is based on $r_{O^{2-}} = 1.40$ Å and is similar to Pauling, Goldschmidt, etc.; the other is based on $r_{F^-} = 1.19$ Å (and $r_{O^{2-}} = 1.26$ Å) and is related to the values determined from X-ray electron density maps. Both sets are comprehensive for cations in different coordination environments but pertain only to oxides and fluorides. We use here the set based on $r_{F^-} = 1.19$ Å (and $r_{O^{2-}} = 1.26$ Å). Radii for some ions M^+ to M^{4+} are shown in Fig. 2.3 as a function of cation coordination number; it should be stressed that the more highly charged ions are unlikely to exist as such but have their positive charge reduced by polarization of the anion and consequent partial covalent bonding between cation and anion. Further data, in the form of bond distances, are given in Appendix 4.

The following trends in ionic radii, with position in the periodic table, formal charge and coordination number, occur:

(a) For the *s*- and *p*-block elements, radii increase with atomic number for any vertical group, e.g. octahedrally coordinated alkali ions.
(b) For any isoelectronic series of cations, radii decrease with increasing charge, e.g. Na^+, Mg^{2+}, Al^{3+} and Si^{4+}.
(c) For any element which can have > 1 oxidation state, the cation radius decreases with increasing oxidation state, e.g. V^{2+}, V^{3+}, V^{4+}, V^{5+}.
(d) For an element which can have various coordination numbers, the cationic radius increases with increasing coordination number.

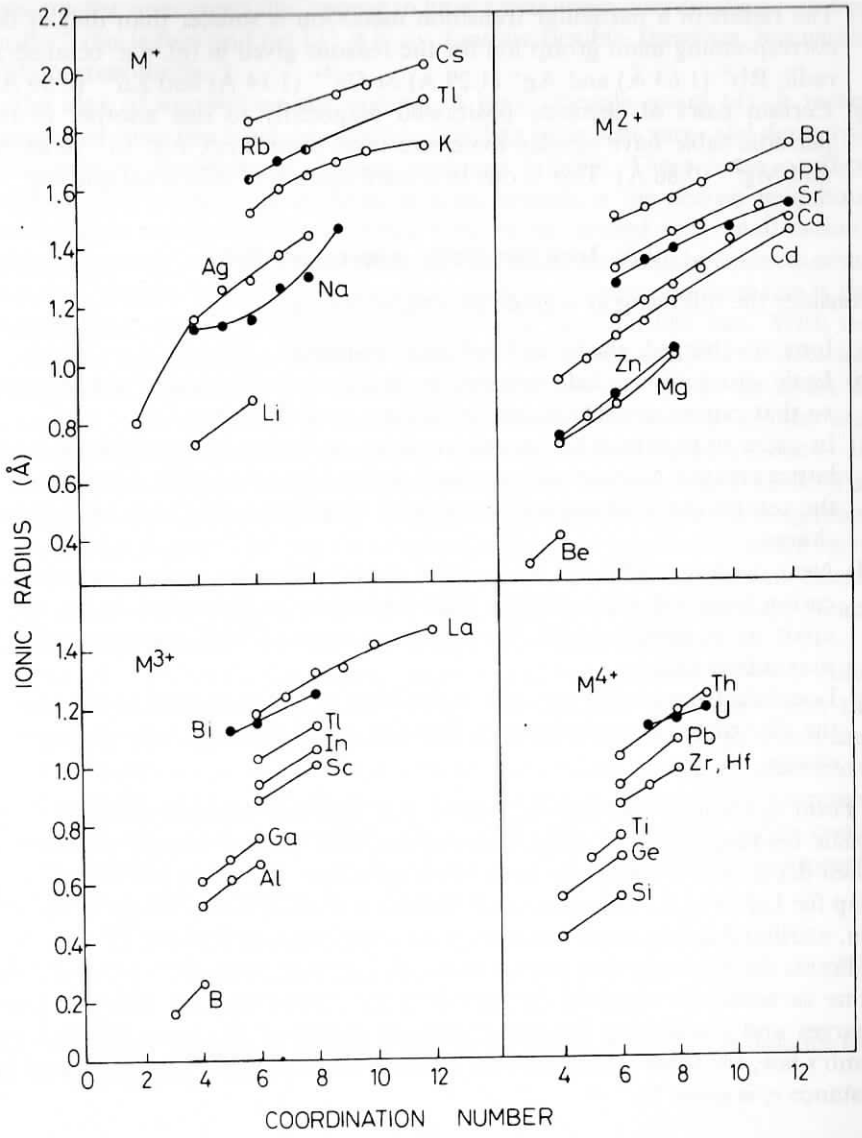

Fig. 2.3 Ionic radii as a function of coordination number for cations M^+ to M^{4+}. (From Shannon and Prewitt, *Acta Cryst.*, **B25**, 725, 1969; **B26**, 1046, 1970. Data based on $r_{F^-} = 1.19$ Å and $r_{O^{2-}} = 1.26$ Å)

(e) In the 'lanthanide contraction', ions with the same charge but increasing atomic number show a reduction in size (due to ineffective shielding of the nuclear charge by the *d* and, especially, *f* electrons), e.g. octahedral radii, La^{3+} (1.20 Å)...Eu^{3+} (1.09 Å)...Lu^{3+} (0.99 Å). Similar effects occur across some series of transition metal ions.

(f) The radius of a particular transition metal ion is smaller than that of the corresponding main group ion for the reasons given in (e), e.g. octahedral radii, Rb^+ (1.63 Å) and Ag^+ (1.29 Å) or Ca^{2+} (1.14 Å) and Zn^{2+} (0.89 Å).
(g) Certain pairs of elements positioned diagonally to one another in the periodic table have similar ionic size (and chemistry), e.g. Li^+ (0.88 Å) and Mg^{2+} (0.86 Å). This is due to a combination of effects (a) and (b).

2.3 Ionic structures—general principles

Consider the following as a guide to ionic structures:

(a) Ions are charged, elastic and polarizable spheres.
(b) Ionic structures are held together by electrostatic forces and are arranged so that cations are surrounded by anions, and vice versa.
(c) In order to maximize the net electrostatic attraction between ions (i.e. the lattice energy), coordination numbers are as high as possible, provided that the central ion 'maintains contact' with its neighbouring ions of opposite charge.
(d) Next nearest neighbour interactions are of the anion–anion and cation–cation type and are repulsive. Like ions arrange themselves to be as far apart as possible and this leads to structures of high symmetry with a maximized volume.
(e) Local electroneutrality prevails; the valence of an ion is equal to the sum of the electrostatic bond strengths between it and adjacent ions of opposite charge.

Point (a) was considered in Section 2.2; ions are obviously charged, are elastic because their size varies with coordination number and are polarizable when departures from purely ionic bonding occurs. Thus, the electron density map for LiF, Fig. 2.1, shows a small distortion from spherical shape of the Li^+ ion, attributable to a small amount of covalent bonding between Li^+ and F^-.

Points (b)–(d) imply that the forces which hold ionic crystals together are the same as would be obtained by regarding the crystal as a 3D array of point charges and considering the net coulombic energy of the array. From Coulomb's law, the force F between two ions of charge Z_+e and Z_-e, separated by distance r, is given by

$$F = \frac{(Z_+e)(Z_-e)}{r^2} \tag{2.1}$$

A similar equation applies to each pair of ions in the crystal and evaluation of the resulting force between all the ions leads to the lattice energy of the crystal (later).

Point (c) includes the proviso that nearest neighbour ions should be 'in contact'. Given the nature of electron density distributions in ionic crystals, it is hard to quantify what is meant by 'in contact'. It is nevertheless important since, although the apparent size of ions varies with coordination number, most

ions, smaller ones especially, appear to have a maximum coordination number; for Be^{2+} this is four and for Li^+ it is six. Ions are flexible, therefore, but within fairly narrow limits.

The idea of *maximizing* the volume of ionic crystals, point (d), is rather unexpected since one is accustomed to regarding ionic structures and derivative *cp* structures, especially, as having *minimum* volume. There is no conflict, however. The prime bonding force in ionic crystals is the nearest neighbour cation–anion *attractive* force and this force is maximized at a small cation–anion separation (when ions become too close, additional repulsive forces come into play, thereby reducing the net attractive force). Superposed on this is the effect of next nearest neighbour *repulsive* forces between like ions. With the constraints that (a) cation–anion distances are minimized and (b) coordination numbers are maximized, like ions arrange themselves to be as far apart as possible in order to reduce their mutual repulsion. This leads to regular and highly symmetrical arrays of ions which tend to have maximized volumes.

An excellent example of a structure whose volume is maximized is rutile. The buckling of the oxide layers, Fig. 1.32(d), causes the next nearest neighbour coordination number of O (by O) to be reduced from 12 (as in *hcp*) to 11 (as in *ptp*). The coordination of Ti by O, and vice versa, is unaffected by this distortion but the overall volume of the structure increases by 2 to 3 per cent. Hence the oxide layers buckle so that the volume can be maximized.

Point (e) is Pauling's *electrostatic valence rule*, the second of a set of rules formulated by Pauling for ionic crystals. Basically, the rule means that the charge on a particular ion, e.g. an anion, must be balanced by an equal and opposite charge on the immediately surrounding cations. However, since these cations are also shared with other anions, it is necessary to estimate the amount of positive charge that is effectively associated with each cation–anion bond. For a cation M^{m+} surrounded by n anions, X^{x-}, the *electrostatic bond strength* (*ebs*) of the cation–anion bonds is defined as

$$ebs = \frac{m}{n} \tag{2.2}$$

For each anion, the sum of the *ebs* of the surrounding cations must balance the charge on the anion, i.e.

$$\sum \frac{m}{n} = x \tag{2.3}$$

For example:

(a) Spinel, $MgAl_2O_4$, contains octahedral Al^{3+} and tetrahedral Mg^{2+} ions; each O is surrounded tetrahedrally by three Al^{3+} ions and one Mg^{2+} ion. We can check that this must be so, as follows:

For Mg^{2+} : $ebs = \frac{2}{4} = \frac{1}{2}$

For Al^{3+} : $ebs = \frac{3}{6} = \frac{1}{2}$

Therefore,

$$\sum ebs(3Al^{3+} + 1Mg^{2+}) = 2$$

(b) We can show that three SiO_4 tetrahedra *cannot* share a common corner in silicate structures:

For Si^{4+} : $ebs = \frac{4}{4} = 1$

Therefore, for an O that bridges two SiO_4 tetrahedra, $\sum ebs = 2$, which is, of course, acceptable. However, three tetrahedra sharing a common O would give $\sum ebs = 3$ for that O, which is quite unacceptable.

This rule of Pauling's provides an important guide to the polyhedral linkages that are and are not possible in crystal structures. Table 2.1 lists some common cations with their formal charge, CN and *ebs*. Table 2.2 lists some allowed and unallowed combinations of polyhedra about a common oxide ion. Many other combinations are possible and the reader may like to deduce some, bearing in mind that there are also topological restrictions on the number of possible

Table 2.1 *Electrostatic bond strengths of some cations*

Cation	Coordination number(s)	*ebs*
Li^+	4, 6	$\frac{1}{4}, \frac{1}{6}$
Na^+	6,8	$\frac{1}{6}, \frac{1}{8}$
Be^{2+}	3,4	$\frac{2}{3}, \frac{1}{2}$
Mg^{2+}	4,6	$\frac{1}{2}, \frac{1}{3}$
Ca^{2+}	8	$\frac{1}{4}$
Zn^{2+}	4	$\frac{1}{2}$
Al^{3+}	4,6	$\frac{3}{4}, \frac{1}{2}$
Cr^{3+}	6	$\frac{1}{2}$
Si^{4+}	4	1
Ge^{4+}	4,6	$1, \frac{2}{3}$
Ti^{4+}	6	$\frac{2}{3}$
Th^{4+}	8	$\frac{1}{2}$

Table 2.2 *Allowed and unallowed combinations of corner-sharing oxide polyhedra*

Allowed	Example	Unallowed
$2SiO_4$tet.	Silica	$> 2SiO_4$tet.
$1MgO_4$tet. + $3AlO_6$oct.	Spinel	$3AlO_4$tet.
$1SiO_4$tet. + $3MgO_6$oct.	Olivine	$1SiO_4$tet. + $2AlO_4$tet.
$8LiO_4$tet.	Li_2O	$4TiO_6$oct.
$2TiO_6$oct. + $4CaO_{12}$dod.	Perovskite	
$3TiO_6$oct.	Rutile	

polyhedral combinations; thus the maximum number of octahedra that can share a common corner is six (as in rock salt), etc.

Pauling's third rule concerns the topology of polyhedra and was considered in Chapter 1. Pauling's first rule states: 'A coordinated polyhedron of anions is formed about each cation; the cation–anion distance is determined by the radius sum and the CN of the cation by the radius ratio'. The idea that cation–anion distances are determined by the radius sum is implicit to every tabulation of ionic radii since a major objective of such tabulations is to be able to predict, correctly, interatomic distances. Let us now consider CNs and *the radius ratio rules*.

2.4 The radius ratio rule

In ideally ionic structures, the CNs of the ions are determined by electrostatic considerations. Cations surround themselves with as many anions as possible, and vice versa. This maximizes the attractions between neighbouring ions of opposite charge and hence maximizes the lattice energy of the crystal (see later). This requirement led to the formulation of the *radius ratio rule* for *ionic structures* in which the ions and the structure adopted for a particular compound depend on the *relative* sizes of the ions. This rule is useful qualitatively but, as we shall see, cannot usually be applied rigorously to explain or predict. There are two guidelines to be followed in using it. First, a cation must be in contact with its anionic neighbours. This places a *lower* limit on the size of cation which may occupy a particular site, since a situation in which a cation may 'rattle' inside its anion polyhedron is assumed to be unstable. Second, neighbouring anions may or may not be in contact. Using these guidelines, one may calculate the range of cation sizes that can occupy the various interstitial sites in an anion array. If you have worked systematically through problems 1.32 to 1.35, then the following section should be a revision.

Let us first calculate the minimum radius for an octahedral cation site, in which both anion–anion and anion–cation contacts occur. The cation is in contact with all six anion neighbours; Fig. 2.4 shows a section through an octahedron, in which the central cation has four coplanar anion neighbours. Applying the Pythagoras theorem,

$$(2r_x)^2 + (2r_x)^2 = [2(r_M + r_x)]^2 \tag{2.4}$$

i.e.

$$2r_x\sqrt{2} = 2(r_M + r_x)$$

and

$$r_M/r_x = \sqrt{2} - 1 = 0.414 \tag{2.5}$$

For radius ratios < 0.414, the cation is too small for an octahedral site and instead, should occupy a site of smaller CN. For radius ratios > 0.414, the

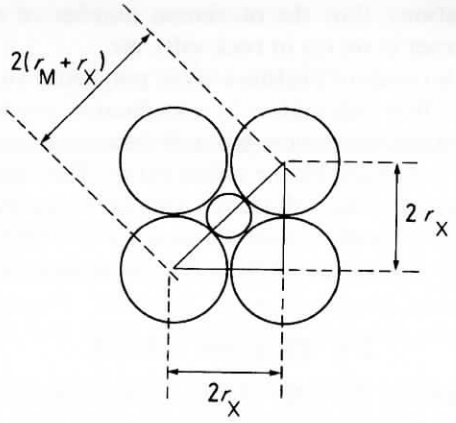

Fig. 2.4 Radius ratio calculation for octahedral coordination

cation would push the anions apart and this happens increasingly up to a radius ratio of 0.732. At this value, the cation can have eight anionic neighbours, all of which are in contact with the cation. To demonstrate this, it is necessary to recognize that cations and anions are in contact along the body diagonal of the cube as in CsCl, Fig. 1.31, i.e.

$$2(r_M + r_x) = (\text{cube body diagonal}) \tag{2.6}$$

In addition, anions are in contact along the cell edge, a, i.e.

$$a = 2r_x \tag{2.7}$$

Therefore,

$$2(r_M + r_x) = 2r_x\sqrt{3}$$

and

$$r_M/r_x = \sqrt{3} - 1 = 0.732 \tag{2.8}$$

In order to evaluate the minimum radius ratio for tetrahedral coordination, we may regard a tetrahedron as a cube with alternate corners missing, Fig. 1.21. Anions and cations are in contact along the cube *body* diagonals, equation (2.6), but anions are in contact along the cube *face* diagonals, i.e.

$$2r_x = (\text{face diagonal}) \tag{2.9}$$

Combining (2.6) and (2.9) and rearranging gives

$$(2r_x)^2 + (\sqrt{2}r_x)^2 = [2(r_M + r_x)]^2$$

i.e.

$$2(r_M + r_x) = \sqrt{6}r_x$$

and

$$r_M/r_x = \frac{\sqrt{6} - 2}{2} = 0.225 \tag{2.10}$$

The minimum radius ratios for various CNs are given in Table 2.3. Note that CN = 5 is absent from the table; in *cp* structures, it is not possible to have a CN of five in which all M—X bonds are of the same length.

The radius ratio rules are successful in predicting trends in CN and structure type but can be used only as a qualitative guide. Radius ratios depend very much on which table of ionic radii is consulted and there appears to be no clear advantage in using either one of the more traditional sets or the modern set of values based on X-ray diffraction results. For example, for RbI, $r+/r- = 0.69$ or 0.80, according to the tables based on $r_{O^{2-}} = 1.40$ and 1.26 Å, respectively. Thus one value would predict six-coordination (rock salt), as observed, but the other predicts eight-coordination (CsCl). On the other hand, LiI has $r+/r- = 0.28$ and 0.46, according to the same tables; one value predicts tetrahedral coordination and the other octahedral (as observed). For the larger cations, especially caesium, $r+/r- > 1$, and it is then more realistic to consider the inverse ratio, $r-/r+$, in for instance, CsF.

A more convincing example of the relevance of radius ratios is provided by oxides and fluorides of general formula MX_2. Possible structure types, with their cation CNs, are silica (4), rutile (6) and fluorite (8). A selection of oxides in each group is given in Table 2.4, together with the radius ratios calculated from Fig. 2.3 (based on $r_{O^{2-}} = 1.26$ Å). Changes in CN are expected at radius ratios of 0.225, 0.414 and 0.732. Bearing in mind that the calculated ratios depend on the table of radii that is used, the agreement between theory and practice is reasonable. For example, GeO_2 is polymorphic and has both silica and rutile structures; the ratio calculated for tetrahedral coordination of Ge is borderline between the values predicted for CN = 4 and 6.

Table 2.3 *Minimum radius ratios*

Coordination	Minimum $r_M : r_x$
Linear, 2	—
Trigonal, 3	0.155
Tetrahedral, 4	0.225
Octahedral, 6	0.414
Cubic, 8	0.732
Dodecahedral, 12	1.000

Table 2.4 *Structures and radius ratios of oxides, MO_2*

Oxide	Calculated radius ratio*		Observed structure type	
CO_2	~0.1	(CN = 2)	Molecular	(CN = 2)
SiO_2	0.32	(CN = 4)	Silica	(CN = 4)
GeO_2	0.43	(CN = 4)	Silica	(CN = 4)
	0.54	(CN = 6)	Rutile	(CN = 6)
TiO_2	0.59	(CN = 6)	Rutile	(CN = 6)
SnO_2	0.66	(CN = 6)	Rutile	(CN = 6)
PbO_2	0.73	(CN = 6)	Rutile	(CN = 6)
HfO_2	0.68	(CN = 6)	Fluorite	(CN = 8)
	0.77	(CN = 8)		
CeO_2	0.75	(CN = 6)	Fluorite	(CN = 8)
	0.88	(CN = 8)		
ThO_2	0.95	(CN = 8)	Fluorite	(CN = 8)

* Since cation radii vary with CN, Fig. 2.3, radius ratios may be calculated for different CNs. The CNs used here are shown in parentheses. Calculations are based on $r_{O^{2-}} = 1.26$ Å.

2.5 Borderline radius ratios and distorted structures

The structural transition from CN = 4 to 6 which occurs with increasing cation size is often clear-cut. Thus GeO_2 has a borderline radius ratio and also exhibits polymorphism. Both polymorphs have highly symmetric structures with CN = 4 and 6 respectively. Polymorphs with CN = 5 do not occur with GeO_2.

In other borderline cases however, distorted polyhedra and/or CNs of 5 are observed. Thus V^{5+} (radius ratio = 0.39 for CN = 4 or 0.54 for CN = 6) has an environment in one polymorph of V_2O_5 which is a gross distortion of octahedral; five V—O bonds are of reasonable length, in the range 1.5 to 2.0 Å, but the sixth is much longer, 2.8 Å, and the coordination is better regarded as distorted square pyramidal. It appears that V^{5+} is rather small to happily occupy an octahedral site and instead, a structure occurs which is transitional between tetrahedral and octahedral. Similar distortions occur between CN = 6 and 8. Thus, ZrO_2 has a borderline radius ratio (0.68 for CN = 6; 0.78 for CN = 8) and although it may have the fluorite structure at very high temperatures (>2000 °C), with CN = 8 for Zr, in its room temperature form as the mineral baddleyite CN = 7 for Zr.

Less severe distortions occur when a cation is only slightly too small for its anion environment. The regular anion coordination is maintained but the cation may rattle or undergo small displacements within its polyhedron. In $PbTiO_3$ (radius ratio for Ti = 0.59 for CN = 6), Ti is displaced by ~ 0.2 Å off the centre of its octahedral site towards a corner oxygen. The direction of displacement is reversible in an applied electric field giving rise to the important property of ferroelectricity (chapter 7).

The concept of 'maximum contact distance' was proposed by Dunitz and Orgel. If the metal–anion distance increases above this distance then the cation is free to rattle. If the metal–anion distance decreases the metal ion is subjected to compression. However, the maximum contact distance does not correspond to the sum of ionic radii, as they are usually defined, and this has been a difficult concept to quantify.

2.6 Lattice energy of ionic crystals

Ionic crystals may be regarded as regular 3D arrays of point charges. The forces that hold them together are entirely electrostatic and may be calculated by summing all the electrostatic repulsions and attractions in the crystal. The *lattice energy, U*, is the net potential energy of the arrangement of charges that forms the structure. It is equivalent to the energy required to sublime the crystal and convert it into a collection of gaseous ions, e.g.

$$NaCl(s) \rightarrow Na^+(g) + Cl^-(g),\ \Delta H = U$$

The value of U depends on the crystal structure, the charge on the ions and the internuclear separation between anion and cation. Two principal kinds of force determine ionic crystal structures:

(a) Electrostatic forces of attraction and repulsion. Two ions M^{Z+} and X^{Z-} separated by a distance, r, experience an attractive force, F, given by Coulomb's law:

$$F = \frac{Z_+ Z_- e^2}{r^2} \tag{2.11}$$

Their coulombic potential energy, V, is given by

$$V = \int_{\infty}^{r} F\mathrm{d}r = -\frac{Z_+ Z_- e^2}{r} \tag{2.12}$$

(b) Short-range repulsive forces which are important when atoms or ions are so close that their electron clouds begin to overlap. Born suggested that this repulsive energy has the form:

$$V = \frac{B}{r^n} \tag{2.13}$$

B is a constant and n is in the range 5 to 12. Because n is large, V falls rapidly to zero with increasing r.

The lattice energy is calculated by combining the net electrostatic attraction and the Born repulsion energies and finding the internuclear separation, r_e, which gives the maximum U value. The procedure is as follows.

Consider the NaCl structure, Fig. 1.24(a). Between each pair of ions there is an electrostatic interaction given by equation (2.11). We wish to sum all such interactions in the crystal and calculate the net attractive energy. Let us first consider one particular ion, e.g. Na^+ in the body centre of the unit cell, and calculate the interaction between it and its neighbours. Its nearest neighbours

are six Cl^- ions in the face centre positions at distance r ($2r$ is the value of the unit cell edge). The attractive potential energy is given by

$$V = -6\frac{e^2 Z_+ Z_-}{r} \tag{2.14}$$

The next nearest neighbours are twelve Na^+ ions at edge centre positions, distance $\sqrt{2}r$; this gives a repulsive potential energy term

$$V = +12\frac{e^2 Z_+ Z_-}{\sqrt{2}r} \tag{2.15}$$

The third nearest neighbours are eight Cl^- ions at the cube corners, distance $\sqrt{3}r$; these are attracted to the central Na^+ ion according to

$$V = -8\frac{e^2 Z_+ Z_-}{\sqrt{3}r} \tag{2.16}$$

The net attractive energy between our Na^+ ion and all other ions in the crystal is given by an infinite series:

$$V = -\frac{e^2 Z_+ Z_-}{r}\left(6 - \frac{12}{\sqrt{2}} + \frac{8}{\sqrt{3}} - \frac{6}{\sqrt{4}} + \cdots\right) \tag{2.17}$$

This summation is repeated for each ion in the crystal, i.e. for $2N$ ions per mole of NaCl. Since each ion pair interaction is thereby counted twice it is necessary to divide the final value by 2, giving

$$V = -\frac{e^2 Z_+ Z_-}{r} NA \tag{2.18}$$

where the *Madelung constant*, A, is the numerical value of the summation in parentheses from equation (2.17). The Madelung constant depends only on the geometrical arrangement of point charges. It has the same value, 1.748, for all compounds with the rock salt structure. Values of A for some other structures are given in Table 2.5.

Table 2.5 *Madelung constants for some simple structures*

Structure type	A
Rock salt	1.748
CsCl	1.763
Wurtzite	1.641
Sphalerite	1.638
Fluorite	2.520
Rutile	2.408

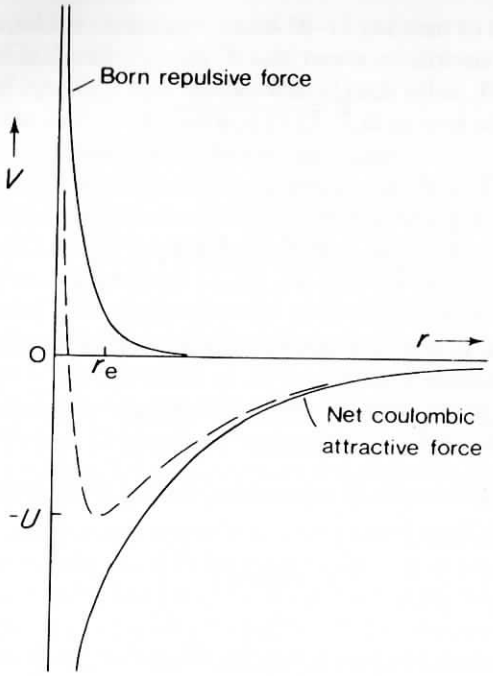

Fig. 2.5 Lattice energy (dashed line) of ionic crystals as a function of internuclear separation

If equation (2.18) were the only factor in the lattice energy, the structure would collapse in on itself since $V \propto -1/r$, equation (2.18) and Fig. 2.5. This catastrophe is avoided by the mutual repulsion between ions, of whatever charge, when they become too close and which is given by equation (2.13). The dependence of this repulsive force on r is shown schematically in Fig. 2.5. The total energy of the crystal, U, is given by summing (2.18) and (2.13) and differentiating with respect to r to find the maximum U value and equilibrium interatomic distance, r_e; i.e.

$$U = -\frac{e^2 Z_+ Z_- NA}{r} + \frac{BN}{r^n} \tag{2.19}$$

Therefore,

$$\frac{dU}{dr} = \frac{e^2 Z_+ Z_- NA}{r^2} - \frac{nBN}{r^{n+1}} \tag{2.20}$$

When

$$\frac{dU}{dr} = 0 \tag{2.21}$$

then

$$B = \frac{e^2 Z_+ Z_- A r^{n-1}}{n} \tag{2.22}$$

and therefore

$$U = -\frac{e^2 Z_+ Z_- NA}{r_e}\left(1 - \frac{1}{n}\right) \tag{2.23}$$

The dashed line in Fig. 2.5 shows the variation of U with r and gives the minimum U value when $r = r_e$.

For most practical purposes, (2.23) is entirely satisfactory, but in more refined treatments certain modifications are made:

(a) The Born repulsive term is represented instead by an exponential function:

$$V = B\exp\left(\frac{-r}{\rho}\right) \tag{2.24}$$

where ρ is a constant, typically 0.35. When r is small ($r \ll r_e$), (2.13) and (2.24) give very different values for V, but for realistic interatomic distances, i.e. $r \simeq r_e$, the two values are similar. Use of equation (2.24) in the expression for U gives the *Born–Mayer equation*:

$$U = -\frac{e^2 Z_+ Z_- AN}{r_e}\left(1 - \frac{\rho}{r_e}\right) \tag{2.25}$$

(b) The zero point energy of the crystal is included in the calculation of U. It equals 2.25 $h\nu_{O_{max}}$, where $\nu_{O_{max}}$ is the frequency of the highest occupied vibrational mode in the crystal. Its inclusion leads to a small reduction in U.

(c) Van der Waals attractive forces exist between ions due to induced dipole-induced dipole interactions. These take the form NC/r^6 and lead to an increase in U.

A more complete equation for U, after correcting for these factors, is

$$U = -\frac{Ae^2 Z_+ Z_- N}{r} + BNe^{-r/\rho} - CNr^{-6} + 2.25Nh\nu_{O_{max}} \tag{2.26}$$

Typical values for the terms, in kJ mol^{-1}, are (from Greenwood):

Substance	$NAe^2Z_+Z_-r^{-1}$	$NBe^{-r/\rho}$	NCr^{-6}	$2.25Nh\nu_{O_{max}}$	U
NaCl	−859.4	98.6	−12.1	7.1	−765.8
MgO	−4631	698	−6.3	18.4	−3921

Thus, the Born repulsive term contributes 10–15 per cent to the value of U; the zero point vibrational and van der Waals terms contribute about 1 per cent each and, being of opposite sign, tend to cancel each other. For most purposes, therefore, we use the simplified equation (2.23). Let us now consider each of the terms in (2.23) and evaluate their relative significance.

The magnitude of U depends on six parameters A, N, e, Z, n and r_e, four of which are constant for a particular structure. This leaves just two, the charge on the ions, Z_+Z_-, and the internuclear separation, r_e. Of the two, charge is the most important since the product (Z_+Z_-) is capable of much larger variation than r_e. For instance, U for a material with divalent ions should be four times as large as for an isostructural crystal with the same r_e but containing monovalent ions (compare the lattice energies of SrO and LiCl, Table 2.6, which have similar r_e, Table 1.7). For isostructural phases with the same Z values but increasing r_e, a decrease in U is expected (e.g. alkali fluorides, alkaline earth oxides with NaCl structure). Lattice energies for materials that show these two trends are given in Table 2.6.

Since U of a crystal is equivalent to its heat of dissociation, a correlation exists between U and the melting point (a better correlation may be sought between U and the sublimation energy, but such data are not so readily available). The effect of (Z_+Z_-) on the melting point is shown by the refractoriness of the alkaline earth oxides (m.p. of CaO = 2572°C) compared with the alkali halides (m.p. of NaCl = 800°C). The effect of r_e on melting points may be seen in series such as:

MgO(2800°C), CaO(2572°C) and BaO(1923°C)

Table 2.6 *Some lattice energies in kJ mol^{-1}; all have rock salt structure.* (Ladd and Lee, *Progr. Solid State Chem.*, **1**, 37–82, 1963; **2**, 378–413, 1965)

MgO	3938	LiF	1024	NaF	911
CaO	3566	LiCl	861	KF	815
SrO	3369	LiBr	803	RbF	777
BaO	3202	LiI	744	CsF	748

2.7 Kapustinskii's equation

Kapustinskii noted an empirical increase in value of the Madelung constant, A, as the CN of the ions increased, e.g. in the series ZnS, NaCl, CsCl, Table 2.5. Since, for a particular anion and cation, r_e also increases with CN, Fig. 2.3, Kapustinskii proposed a general equation for U in which variations in A and r_e are auto-compensated. He suggested using the rock salt value for A and octahedral ionic radii (Goldschmidt) in calculating r_e; substituting $r_e = r_c + r_a$, $\rho = 0.345$, $A = 1.745$ and values for N and e into equation (2.25) gives the Kapustinskii equation:

$$U = \frac{1200.5VZ_+Z_-}{r_c + r_a}\left(1 - \frac{0.345}{r_c + r_a}\right)\text{kJ mol}^{-1} \tag{2.27}$$

Table 2.7 *Thermochemical radii (Å) of complex anions.* (Kapustinskii, *Quart. Rev.*, 283–294, 1956)

BF_4^-	2.28	CrO_4^{2-}	2.40	IO_4^-	2.49
SO_4^{2-}	2.30	MnO_4^-	2.40	MoO_4^{2-}	2.54
ClO_4^-	2.36	BeF_4^-	2.45	SbO_4^{3-}	2.60
PO_4^{3-}	2.38	AsO_4^{3-}	2.48	BiO_4^{3-}	2.68
OH^-	1.40	O_2^{2-}	1.80	CO_3^{2-}	1.85
NO_2^-	1.55	CN^-	1.82	NO_3^-	1.89

where V is the number of ions per formula unit (two in NaCl, three in PbF_2, etc.). This formula may be used to calculate U of any known or hypothetical ionic compound and in spite of the assumptions involved, the answers obtained are surprisingly accurate.

The Kapustinskii equation was used to predict the stable existence of several previously unknown compounds. In cases where U was known from Born–Haber cycle calculations (see later), it was used to derive values for ionic radii. This has been particularly useful for complex anions, e.g. SO_4^{2-}, PO_4^{3-}, whose effective size in crystals is difficult to measure by other means. Radii determined in this way are known as *thermochemical radii*; some values are given in Table 2.7. It should be noted that radii for non-spherical ions such as CN^- represent gross simplifications and are really applicable only to other lattice energy calculations.

2.8 The Born–Haber cycle and thermochemical calculations

The lattice energy of a crystal is equivalent to its heat of formation from one mole of its ionic constituents in the gas phase:

$$Na^+(g) + Cl^-(g) \rightarrow NaCl(s), \quad \Delta H = U$$

It cannot be measured experimentally. However, the heat of formation of a crystal, ΔH_f, can be measured relative to the reagents in their standard states:

$$Na(s) + \frac{1}{2}Cl_2(g) \rightarrow NaCl(s), \quad \Delta H = \Delta H_f$$

ΔH_f may be related to U by constructing a thermochemical cycle known as a Born–Haber cycle, in which ΔH_f is given by the summation of energy terms in a hypothetical reaction pathway. For NaCl, the individual steps in the pathway, commencing with the elements in their standard states, are:

Sublimation of solid Na	$\Delta H = S$
Ionization of gaseous Na atoms	$\Delta H = \text{IP}$
Dissociation of Cl_2 molecules	$\Delta H = \frac{1}{2}D$
Formation of the Cl^- ion	$\Delta H = \text{EA}$
Coalescence of gaseous ions to give crystalline NaCl	$\Delta H = U$

Addition of these five terms is equivalent to forming crystalline NaCl from solid Na and gaseous Cl_2, as shown:

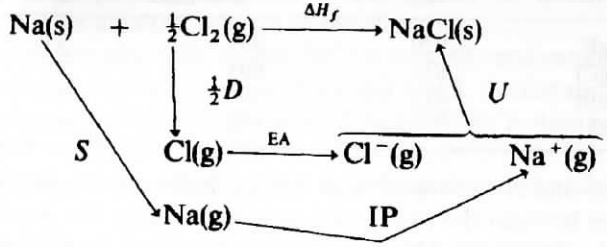

From Hess' Law,

$$\Delta H_f = S + \frac{1}{2}D + \text{IP} + \text{EA} + U \qquad (2.28)$$

Applications. The Born–Haber cycle and equation (2.28) have various uses:

(a) Six enthalpy terms are present in equation (2.28). If all six can be determined independently, then the cycle gives a check on internal consistency of the data. The values (in kJ mol^{-1}) for Nacl are:

S	109
IP	493.7
$\frac{1}{2}D$	121
EA	−356
U	−764.4
ΔH_f	−410.9

Summation of the first five terms gives a calculated H_f of −396.7 kJ mol^{-1}, which compares reasonably well with the measured ΔH_f value of −410.9 kJ mol^{-1}.

(b) If only five of the terms are known, the sixth may be evaluated using equation (2.28). An early application was in the calculation of electron affinities, for which data were not then available.

(c) The stability of an unknown compound may be estimated. It is necessary to assume a structure in order to calculate U; while there are obviously errors involved, e.g. in choosing r_e, these are usually unimportant compared with the effect of some of the other energy terms in equation (2.28). Having estimated U, ΔH_f may be calculated. If ΔH_f is large and positive, it is clear why the compound is unknown—it is unstable relative to its elements. If ΔH_f (calc.) is negative, however, it may be worthwhile to try and prepare the compound under certain conditions. Examples are given in the next section.

(d) Differences between U values obtained by the Born–Haber cycle and calculated from an ionic model of the crystal structure may be used as evidence for non-ionic bonding effects. Data for the silver halides,

Table 2.8 *Lattice energies (kJ mol^{-1}) of Group I halides.* (Waddington, *Adv. Inorg. Chem. Radiochem.*, **1**, 157–221, 1959)

	U_{calc}	$U_{Born-Haber}$	ΔU
AgF	920	953	33
AgCl	832	903	71
AgBr	815	895	80
AgI	777	882	105

Table 2.8, and for thallium and copper halides (not given) show that differences between the two lattice energies are least for the fluorides and greatest for the iodides. This is attributed to covalent bonding in the iodides leading to an increase in thermochemical lattice energy values. A correlation also exists between the insolubility of the Ag salts, especially AgI, in water and the presence of partial covalent bonding. Data for the corresponding alkali halides show that differences between thermochemical and calculated lattice energies are small; therefore, the ionic bonding model may be applied satisfactorily to them.

While covalent bonding is present in AgCl and AgBr, it is not strong enough to change the crystal structure from that of rock salt to one of lower CN. AgI is different, however; it is polymorphic and exists in at least three structure types, all of which have low CNs, usually four. Changes in structure and CN due to increased covalent bonding are described later.

(e) Certain transition elements have *crystal field stabilization energies*, CFSE, due to their *d* electron configuration and this gives an increased lattice energy in their compounds. For example, the difference between experimental and calculated *U* in CoF_2 is 83 kJ mol^{-1}, in fair agreement with the CFSE value calculated for the high spin state of Co in CoF_2 of 104 kJ mol^{-1}. Ions which do not exhibit CFSE effects have the configurations d^0 (e.g. Ca^{2+}), d^5 high spin (e.g. Mn^{2+}) and d^{10} (e.g. Zn^{2+}).

(f) The Born–Haber cycle has many other uses, e.g. in solution chemistry to determine energies of complexation and hydration of ions. These usually require knowledge of the lattice energy of the appropriate solids, but since they do not provide any new information about solids, they are not discussed further.

2.9 Stabilities of real and hypothetical ionic compounds

a) Inert gas compounds

One may ask, whether it is worthwhile trying to synthesize, for example, ArCl. Apart from ΔH_f, the only unknown in equation (2.28) is *U*. Suppose that hypothetical ArCl had the rock salt structure and the radius of the Ar^+ ion is between that of Na^+ and K^+. An estimated lattice energy for ArCl is, then, −745 kJ mol^{-1} (NaCl = −764.4; KCl = −701.4). Substitution in (2.28) gives, in kJ mol^{-1}:

S	$\frac{1}{2}D$	IP	EA	*U*	ΔH_f (calc.)
0	121	1524	−356	−745	+544

ArCl has a large positive ΔH_f (calc) and would be thermodynamically unstable, by a large amount, relative to the elements.

Such a calculation also tells us *why* ArCl is unstable and cannot be synthesized. Comparing the calculations for ArCl and NaCl, the instability of ArCl is due to the very high ionization potential of Ar (stability is strictly governed by free energies of formation, but ΔS is small and hence $\Delta G \simeq \Delta H$). The heats of formation calculated for several other hypothetical compounds are given in Table 2.9.

A large number of inert gas compounds are now known, following the preparation of $XePtF_6$ by Bartlett in 1962. Consideration of lattice energies and enthalpies of formation led Bartlett to try and synthesize $XePtF_6$ by direct reaction of Xe and PtF_6 gases. He had previously prepared O_2PtF_6 as an ionic salt, $(O_2)^+(PtF_6)^-$, by reacting (by accident) O_2 with PtF_6. From a knowledge of the similarity in the first ionization potentials of molecular oxygen (1176 kJ mol^{-1}) and xenon (1169 kJ mol^{-1}), he reasoned, correctly, that the corresponding Xe compound should be stable.

Table 2.9 *Enthalpies of formation (kJ mol^{-1}) of some hypothetical (*) and real compounds*

HeF^*	+1066	$NeCl^*$	+1028	$CsCl_2^*$	+213	CuI_2	−21
ArF^*	+418	NaCl	−411	CsF_2^*	−125	$CuBr_2$	−142
XeF^*	+163	$MgCl^*$	−125	AgI_2^*	+280	$CuCl_2$	−217
$MgCl_2$	−639	$AlCl^*$	−188	$AgCl_2$	+96	CuF_2	−890
$NaCl_2^*$	+2144	$AlCl_3$	−694	AgF_2	−205		

b) Lower and higher valence compounds

Consider alkaline earth compounds. In these, the metal is always divalent. Since a great deal of extra energy is required to doubly ionize the metal atoms, it is reasonable to ask why monovalent compounds, such as 'MgCl', do not form. Data in Table 2.9 show that MgCl is indeed stable relative to the elements (ΔH(calc.) = −125 kJ mol^{-1}) but that $MgCl_2$ is much more stable (ΔH = −639 kJ mol^{-1}). This is shown by the following sequence of enthalpies:

$$2Mg + Cl_2 \xrightarrow{-250} 2MgCl \xrightarrow{-389} Mg + MgCl_2$$
$$2Mg + Cl_2 \xrightarrow{\qquad -639 \qquad} Mg + MgCl_2$$

In any attempt to synthesize MgCl, attention should be directed towards keeping the reaction temperature low and/or isolating the MgCl product, in order to prevent it from reacting further or disproportionating. Similar trends are observed for other hypothetical compounds such as ZnCl, Zn_2O, AlCl and $AlCl_2$.

From a consideration of the factors that affect the stability of compounds, the following conclusions may be drawn about compounds with metals in unusual oxidation states:

(a) The formation and stability of compounds with lower than normal valence states is favourable when (i) the second, and higher, ionization potentials of the metal are particularly high and (ii) the lattice energy of the corresponding compounds with the metal in its normal oxidation state is reduced.
(b) In order to prepare compounds with the metal in a higher than normal oxidation state and during which it may be necessary to break into a closed electron shell, it is desirable to have (i) low values for the second (or higher) ionization potential of the metal atoms and (ii) large lattice energies of the resulting higher valence compounds.

As examples of these trends, calculations for the alkaline earth monohalides show that while all are unstable relative to the dihalides, the enthalpy of disproportionation is least in each case for the iodide ($U_{(MI_2)} < U_{(MBr_2)}$, etc.—effect a, ii). On the other hand, higher valence halogen compounds of the Group I elements are most likely to occur with caesium and the copper subgroup elements (effect b, i), in combination with fluorine (effect b, ii). Thus, from Table 2.9, all caesium dihalides, apart from CsF_2, have positive ΔH_f values and would be unstable. CsF_2 is stable in principle, with its negative ΔH_f value, but has not been prepared because its disproportionation to CsF has a large negative ΔH:

$$Cs + F_2 \xrightarrow{-125} CsF_2 \xrightarrow{405} CsF + \tfrac{1}{2}F_2 \qquad (-530)$$

For the silver dihalides, ΔH_f becomes less positive and finally negative across the series AgI_2 to AgF_2. This again shows the effect of r_e on U and hence on ΔH_f (effect b, ii). Unlike CsF_2, AgF_2 is stable since AgF and AgF_2 have similar enthalpies of formation and the disproportionation enthalpy of AgF_2 (to AgF $+\frac{1}{2}F_2$) is approximately zero.

The copper halides are particularly interesting. The divalent state of copper, in which the d^{10} shell of copper is broken into, is the most common state and again the dihalides show decreasing stability across the series CuF_2 to CuI_2, Table 2.9: CuI_2 appears not to exist and its calculated ΔH_f is barely negative. In the monovalent state the situation is reversed and all the halides apart from CuF are known. CuF is calculated to be stable relative to the elements but not relative to CuF_2:

$$2Cu + F_2 \xrightarrow{-36} 2CuF \xrightarrow{-91} CuF_2 + Cu \qquad (-127)$$

These examples show that several factors affect the formulae and stability of compounds: ionization potentials, lattice energies (via internuclear distances and ionic charges) and the relative stability of elements in different oxidation states. Often a delicate balance between opposing factors controls the stability or instability of a compound and, as with the copper halides, detailed calculations are needed to assess the factors involved.

2.10 Partial covalent bonding

Covalent bonding, partial or complete, occurs when the outer electronic charge density on an anion is polarized towards and by a neighbouring cation. The net effect is that an electron pair which would be associated entirely with the anion in a purely ionic structure is displaced to occur between the anion and cation. In cases of partial covalent bonding, some electron density is common to both atoms but the rest is associated with the more electronegative atom.

Some clear-cut examples of the influence of bonding type on crystal structure are as follows:

(a) *SrO, BaO, HgO.* SrO and BaO both have the rock salt structure with octahedral M^{2+} ions. Based on size considerations alone, and if it were ionic, HgO should have the same structure. However, mercury is only *two* coordinate in HgO; linear O–Hg–O segments occur and may be rationalized on the basis of *sp* hybridization of mercury. The ground state of atomic mercury is

$$(\text{Xe core})\quad 4f^{14}\quad 5d^{10}\quad 6s^2$$

The first excited state, corresponding to mercury (II), is

$$(\text{Xe core})\ 4f^{14}\quad 5d^{10}\quad 6s^1\quad 6p^1$$

Hybridization of the 6*s* and one 6*p* orbital gives rise to two, linear *sp* hybrid orbitals, each of which forms a normal, electron pair covalent bond by overlap with an orbital on oxygen. Hence mercury has a CN of two in HgO.

(b) $AlF_3, AlCl_3, AlBr_3, AlI_3$. These show a smooth transition from ionic to covalent bonding as the electronegativity difference between the two elements decreases. Thus, AlF_3 is a high melting, essentially ionic solid with a distorted octahedral coordination of Al^{3+} ions; its structure is related to that of ReO_3. $AlCl_3$ has a layered, polymeric structure in the solid state similar to that of $CrCl_3$, which is related to the $CdCl_2$ and CdI_2 structures. The bonds may be regarded as part ionic/part covalent. $AlBr_3$ and AlI_3 have molecular structures with dimeric units of formula Al_2X_6. Their structure and shape are shown in Fig. 1.20 and the bonding between Al, and Br, or I is essentially covalent.

Halides of other elements, e.g. Be, Mg, Ga, In, also show variations in bond type and structure, depending on the halide. The trends are always the same; the fluorides have the largest difference in electronegativity between the two elements and their structures are the most ionic. Increasing covalent character

occurs in the series, chloride—bromide—iodide. The occurrence of partial covalent bonding in an otherwise ionic structure may sometimes be detected by abnormally large values of the lattice energy, Table 2.8. In others, it is clear from the nature of the structure and the coordination numbers of the atoms that the bonding cannot be purely ionic.

It is still difficult to quantify the degree of partial covalence in a particular structure, although chemists intuitively feel most so-called ionic structures must have a considerable degree of covalent character. Two approaches which have had considerable success in quantifying ionicity or partial covalent bonding are the coordinated polymeric model of Sanderson and the ionicity plots of Mooser and Pearson.

2.11 Coordinated polymeric structures—Sanderson's model

Sanderson regards all bonds in non-molecular structures as polar covalent. The atoms contain partial charges whose values may be calculated readily using a scale of electronegativities developed by Sanderson. From the partial charges, the relative contributions of ionic and covalent bonding to the total bond energy may be estimated. Since all non-molecular crystals contain partially charged atoms, the ionic model represents an extreme form of bonding that is not attained in practice. Thus in KCl, the charges on the atoms are calculated to be ± 0.76 instead of ± 1.0 for a purely ionic structure.

The essential features of an atom which control its physical and chemical properties are (a) its electronic configuration and (b) the effective nuclear charge felt by the valence electrons. Recognition of the importance of the latter effect provides the starting point for Sanderson's model.

a) Effective nuclear charge

The *effective nuclear charge* of an atom is the positive charge that would be felt by a foreign electron on arriving at the periphery of the atom. Atoms are, of course, electrically neutral overall but, nevertheless, the valence electrons are not very effective in shielding the outside world from the positive charge on the nucleus. Consequently, an incoming electron (e.g. an electron that belongs to a neighbouring atom and is coming to investigate the possibility of bond formation) feels a positive, attractive charge. Were this not the case and the surface of an atom were completely shielded from the nuclear charge, then atoms would have zero *electron affinity* and no bonds, ionic or covalent, would ever form.

The effective nuclear charge is greatest in elements which have a single vacancy in their valence shell, i.e. in the halogens. In the inert gases, the outermost electron shell is full and no foreign electrons can enter it. Consequently, incoming electrons would have to occupy vacant orbitals which are essentially 'outside' the atom and the effective nuclear charge experienced in such orbitals would be greatly reduced. Calculations of *screening constants* were made by Slater who found that outermost electrons are much less efficient at screening nuclear charge than are electrons in inner shells. The screening

constants of outermost electrons are calculated to be approximately one third; this means that for each unit increase in atomic number and positive nuclear charge across a series, e.g. from sodium to chlorine, the additional positive charge is screened by only one third. Therefore, the effective nuclear charge increases in steps of two thirds and the valence electrons experience an increasingly strong attraction to the nucleus on going from sodium to chlorine. Similar effects occur throughout the periodic table: the effective nuclear charge is small for the alkali metals and increases to a maximum in the halogens.

Many atomic properties correlate with effective nuclear charge:

(a) Ionization potentials increase from left to right across the periodic table.
(b) Electron affinities become increasingly negative in the same direction.
(c) Atomic radii decrease from left to right.
(d) Electronegativities increase from left to right.

Let us consider two of these, atomic radii and electronegativities, in more detail.

b) Atomic radii

Atomic radii vary considerably for a particular atom depending on bond type and CN and many tabulations of radii are available; indeed, the subject of ionic radii is still controversial. Fortunately, *non-polar covalent radii* can be measured accurately and represent a point of reference with which to compare other radii. Thus the atomic, non-polar covalent radius of carbon, given by half the C—C single bond length, is constant at 0.77 Å in materials as diverse as diamond and gaseous hydrocarbons. Non-polar radii, r_c, are listed in Table 2.10; from these, it is possible to estimate the effect that partial charges on atoms have on their radii. The general trends are that with increasing amounts of partial positive charge, the radii become smaller (i.e. as electrons are removed from the valence shell, but with the nuclear charge unchanged, the remaining valence shell electrons feel a stronger attraction to the nucleus and the atom contracts). Conversely, with increasing negative charge on the atom, the radius becomes larger. Sanderson developed a simple, empirical formula to quantify the variation of radius, r, with partial charge:

$$r = r_c - B\delta \tag{2.29}$$

where r_c is the non-polar covalent radius, B is a constant for a particular atom and δ is its partial charge. B values are also given in Table 2.10. The partial charges on atoms cannot be measured directly but may be estimated from Sanderson's electronegativity scale, as follows.

c) Electronegativity and partially charged atoms

The electronegativity of an atom is a measure of the net attractive force experienced by an outermost electron towards the nucleus. Electronegativity,

Table 2.10 *Some electronegativity and size parameters of atoms. (After Sanderson, 1976)*

Element	S^*	r_c (Å)†	B (solid)‡	ΔS_c §	r_i (Å)¶
H	3.55	0.32		3.92	
Li	0.74	1.34	0.812	1.77	0.53
Be	1.99	0.91	0.330	2.93	0.58
B	2.93	0.82		2.56	
C	3.79	0.77		4.05	
N	4.49	0.74		4.41	
O	5.21	0.70	4.401	4.75	1.10
F	5.75	0.68	0.925	4.99	1.61
Na	0.70	1.54	0.763	1.74	0.78
Mg	1.56	1.38	0.349	2.60	1.03
Al	2.22	1.26		3.10	
Si	2.84	1.17		3.51	
P	3.43	1.10		3.85	
S	4.12	1.04	0.657	4.22	1.70
Cl	4.93	0.99	1.191	4.62	2.18
K	0.42	1.96	0.956	1.35	1.00
Ca	1.22	1.74	0.550	2.30	1.19
Zn	2.98			3.58	
Ga	3.28			3.77	
Ge	3.59	1.22		3.94	
As	3.90	1.19		4.11	
Se	4.21	1.16	0.665	4.27	1.83
Br	4.53	1.14	1.242	4.43	2.38
Rb	0.36	2.16	1.039	1.25	1.12
Sr	1.06	1.91	0.429	2.14	1.48
Ag	2.59	1.50	0.208		1.29
Cd	2.84	1.46	0.132	3.35	1.33
Sn	3.09	1.40		3.16, 3.66	
Sb	3.34	1.38		3.80	
Te	3.59	1.35	0.692	3.94	2.04
I	3.84	1.33	1.384	4.08	2.71
Cs	0.28	2.35	0.963	1.10	1.39
Ba	0.78	1.98	0.348	1.93	1.63
Hg	2.93			3.59	
Tl	3.02	1.48		2.85	
Pb	3.08	1.47		3.21, 3.69	
Bi	3.16	1.46		3.74	

* Sanderson's electronegativity.
† Non-polar covalent radii.
‡ Constant in equation (2.29) relating size to partial charge.
§ Charge in electronegativity on acquiring unit charge.
¶ Radii calculated for singly charged ions.

originated by Pauling, is a parameter that correlates with the polarity of bonds between unlike atoms. Atoms of high electronegativity attract electrons (in a covalent bond) more than do atoms of low electronegativity and, hence, they acquire a partial negative charge. The magnitude of the partial charge depends on the initial difference in electronegativity between the two atoms. Pauling

observed a correlation between the strengths of polar bonds and the degree of polarity in the bonds. He proposed that bond strengths are a combination of (a) a homopolar bond energy and (b) an 'extra ionic energy' due to bond polarity and, hence, electronegativity difference. He then used this correlation between polarity and extra ionic energy to establish a scale of electronegativities. These ideas were modified by Sanderson using a different method to derive a scale of electronegativities; this then allowed quantitative calculations of bond energies for a wide variety of compounds. Since electronegativity is a measure of the attraction between the effective nuclear charge and an outermost electron, it is related to the compactness of an atom. The relation:

$$S = \frac{D}{D_a} \tag{2.30}$$

is used to evaluate the electronegativity, S, in which D is the electron density of the atom (given by the ratio of atomic number:atomic volume) and D_a is the electron density that would be expected for the atom by linear interpolation of the D values for the inert gas elements. The electronegativity values so obtained are listed in Table 2.10, with some minor modifications made by Sanderson.

An important contribution to our understanding of bond formation is *the principle of electronegativity equalization*. It may be stated: 'When two or more atoms initially different in electronegativity combine chemically, they adjust to have the same intermediate electronegativity within the compound.' The value of the intermediate electronegativity is given by the geometric mean of the individual electronegativities of the component atoms, e.g. for NaF:

$$S_b = \sqrt{S_{Na} S_F} = 2.006 \tag{2.31}$$

Thus, in a bond between unlike atoms, the bonding electrons are preferentially and partially transferred from the less electronegative to the more electronegative atom. The resulting partial negative charge on the more electronegative atom is defined as follows: '*Partial charge* is the ratio of the change in electronegativity undergone by an atom on bond formation to the change it would have undergone on becoming completely ionic with charge + or −1.'

In order to calculate partial charges, a point of reference is necessary; for this it is assumed that the bonds in NaF are 75 per cent ionic; it is also assumed that electronegativity changes linearly with charge. It can then be shown that the change in electronegativity, ΔS_c, of an atom on acquiring a unit positive or negative charge is given by

$$\Delta S_c = 2.08\sqrt{S} \tag{2.32}$$

Partial charge, δ, is defined as

$$\delta = \frac{\Delta S}{\Delta S_c} \tag{2.33}$$

where $\Delta S = S - S_b$. Values of ΔS_c are also given in Table 2.10.

Returning now to the radii of partially charged atoms, the problem in assigning radii to atoms or ions is how to divide an experimentally observed internuclear distance into its component radii. Many methods have been tried and various tabulations of radii are available. All are additive in that they correctly predict bond distances. The method adopted by Pauling (and Sanderson) has been to divide the experimental internuclear distance in an isoelectronic 'ionic' crystal, such as NaF, according to the inverse ratio of the effective nuclear charges on the two 'ions'. Effective nuclear charges can be calculated from the screening constants. From the partial charges on the atoms and assuming that radii change systematically with partial charge (according to the relation $r = r_c - B\delta$), the ionic radii of Na^+ and F^- may be calculated; these then serve as a point of reference for calculating radii of other ions in materials that are not isoelectronic. In Table 2.10 are listed the radii of singly charged ions in the solid state calculated by this method; also given are B and r_c data to enable radii to be calculated and electronegativity data S, ΔS_c to enable partial charges, δ, to be calculated.

Let us use these data for one example, BaI_2. From Table 2.10, $S_{Ba} = 0.78$ and $S_I = 3.84$; the intermediate electronegativity, S_b, is given by $S_b = \sqrt[3]{S_{Ba} S_I^2} = 2.26$. Therefore, for Ba $\Delta S = 2.26 - 0.78 = 1.48$ and for iodine, $\Delta S = 3.84 - 2.26 = 1.58$. The values of ΔS_c are 1.93 (Ba) and 4.08 (I). Hence $\delta_{Ba} = 1.48/1.93 = 0.78$ and $\delta_I = 1.58/4.08 = -0.39$, i.e. BaI_2 is ~ 39 per cent ionic, 61 per cent covalent (using the δ_I value). The radii of the partially charged atoms may now be calculated. For Ba, $r_c = 1.98$, $B = 0.348$ and δ is calculated to be 0.78; hence $r_{Ba} = r_c - B\delta = 1.71$ Å. For I, $r_c = 1.33$, $B = 1.384$ and $\delta = -0.39$; hence $r_I = 1.87$ Å. Therefore, the Ba–I distance is calculated to be $1.87 + 1.71 = 3.58$ Å, close to the experimental value of 3.59 Å.

Using these methods, Sanderson evaluated the partial charges and atomic radii in a large number of solid compounds. Data are given in Table 2.11 for a number of mono- and divalent chlorides; the charge on Cl varies from −0.21 in $CdCl_2$ to −0.81 in CsCl; at the same time the calculated radius varies from 1.24 to 1.95 Å. These compare with a non-polar covalent radius of 0.99 Å and an ionic radius of 2.18 Å, Table 2.10. While these radii and partial charges may not be quantitatively correct, because some of the assumptions involved in their calculation are rather empirical, they nevertheless appear to be realistic. Most of the compounds in Table 2.11 are normally regarded as ionic, and if the partial charge data are in any way correct, they clearly show that it is unrealistic and misleading to assign a radius to the chloride ion which is constant for all solid chlorides.

A similar but more extensive list of the partial charges on oxygen in a variety of oxides is given in Table 2.12, where values cover almost the entire range between 0 and −1. Although oxides are traditionally regarded as containing the oxide ion, O^{2-}, calculations show that the actual charge carried by an oxygen never exceeds −1 and is usually much less than −1. This is, of course, consistent with electron affinity data for oxygen. Although these are *gas phase* data, it is clear that while the reaction, $O + e \rightarrow O^-$ is exothermic, $O^- + e \rightarrow O^{2-}$ is endothermic and therefore, unfavourable.

Table 2.11 *Partial charge and radius of the chlorine atom in some solid chlorides*

Compound	$-\delta_{Cl}$	r_{Cl} (Å)	Compound	$-\delta_{Cl}$	r_{Cl}(Å)
$CdCl_2$	0.21	1.24	$BaCl_2$	0.49	1.57
$BeCl_2$	0.28	1.26	LiCl	0.65	1.76
CuCl	0.29	1.34	NaCl	0.67	1.79
AgCl	0.30	1.35	KCl	0.76	1.90
$MgCl_2$	0.34	1.39	RbCl	0.78	1.92
$CaCl_2$	0.40	1.47	CsCl	0.81	1.95
$SrCl_2$	0.43	1.50			

Table 2.12 *Partial charge on oxygen in some solid oxides*

Compound	$-\delta_O$	Compound	$-\delta_O$	Compound	$-\delta_O$	Compound	$-\delta_O$
Cu_2O	0.41	BeO	0.36	BaO	0.68	La_2O_3	0.56
Ag_2O	0.41	PbO	0.36	Ga_2O_3	0.19	CO_2	0.11
Li_2O	0.80	SnO	0.37	Tl_2O_3	0.21	GeO_2	0.13
Na_2O	0.81	FeO	0.40	In_2O_3	0.23	SnO_2	0.17
K_2O	0.89	CoO	0.40	B_2O_3	0.24	PbO_2	0.18
Rb_2O	0.92	NiO	0.40	Al_2O_3	0.31	SiO_2	0.23
Cs_2O	0.94	MnO	0.41	Fe_2O_3	0.33	MnO_2	0.29
HgO	0.27	MgO	0.50	Cr_2O_3	0.37	TiO_2	0.39
ZnO	0.29	CaO	0.56	Sc_2O_3	0.47	ZrO_2	0.44
CdO	0.32	SrO	0.60	Y_2O_3	0.52	HfO_2	0.45
CuO	0.32						

From the principle of electronegativity equalization, electrons in a hypothetical covalent bond are partially transferred to the more electronegative atom. This removal of electrons from the electropositive atom leads to an increase in its effective nuclear charge, decrease in its size and hence an increase in its effective electronegativity. Likewise, as the electronegative atom acquires electrons, so its ability to attract still more electrons diminishes and its electronegativity decreases. In this way the electronegativities of the two atoms adjust themselves until they are equal. This principle of electronegativity equalization may be applied equally to diatomic gas molecules, in which only one bond is involved, or to 3D solid structures in which each atom is surrounded by and bonded to several others. It illustrates how covalent bonds that are initially non-polar may become polar due to electronegativity equalization.

An alternative approach is to start with purely ionic bonds and consider how they may acquire some covalent character. In an ionic structure, M^+X^-, the cations are surrounded by anions (usually 4, 6 or 8). However, the cations have empty valence shells and are potential electron pair acceptors; likewise, anions with their filled valence shells are potential electron pair donors. The cations and anions therefore interact in the same way as do Lewis acids and bases: the anions, with their lone pairs of electrons, coordinate to the surrounding cations. The strength of this interaction, and hence the degree of covalent bonding which results, is again related to the electronegativities of the two atoms.

Thus electronegative cations such as Al^{3+} are much stronger electron pair acceptors (and Lewis acids) than are electropositive cations such as K^+. The *coordinated polymeric model* of structures, proposed by Sanderson, is based on this idea of acid–base interactions between ions. It therefore forms a bridge between the ionic and covalent extremes of bond type.

2.12 Mooser–Pearson plots and ionicities

While the radius ratio rules are rather unsatisfactory for predicting the structure adopted by, for instance, particular AB compounds, an alternative approach by Mooser and Pearson has had considerable success. This focuses on the directionality or covalent character of bonds. The two factors regarded as influencing covalent bond character in crystals are (a) the average principal quantum number, $\bar{n}$, of the atoms involved and (b) their difference in electronegativity, Δx. In constructing Mooser–Pearson plots, these two parameters are plotted against each other, as shown for AB compounds in Fig. 2.6. The most striking feature is the clean separation of compounds into four groups corresponding to the structures: zinc blende (ZnS, B), wurtzite (ZnS, W), rock salt and CsCl. One's intuitive feeling is that zinc blende (or sphalerite) is the most covalent and either rock salt or CsCl is the most ionic. Mooser–Pearson plots present this intuitive feeling in diagrammatic form.

The ionic character in the bonds, termed *ionicity*, increases from the bottom left to the top right of the diagram, as shown by the arrow. Thus ionicity is not governed by electronegativity alone but also depends on the principal valence shell of the atoms and hence on atomic size. There is a general trend for highly directional covalent bonds to be associated with light elements, i.e. at the bottom of Fig. 2.6, and with small values of Δx, i.e. at the left-hand side of Fig. 2.6.

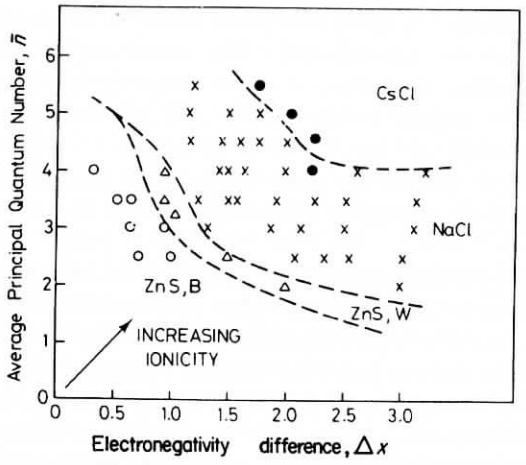

Fig. 2.6 Mooser–Pearson plot for AB compounds containing A group cations (*Acta Cryst.*, **12**, 1015, 1959). Arrow indicates direction of increasing bond ionicity

The fairly sharp crossover between the different '*structure fields*' in Fig. 2.6 suggests that for each structure type there are critical ionicities which place a limit on the compounds that can have that particular structure. Theoretical support for Mooser–Pearson plots has come from the work of Phillips and van Vechten who measured optical absorption spectra of some AB compounds and, from these, calculated electronegativities and ionicities. The spectral data gave values of band gaps, E_g (see later). For isoelectronic series of compounds, e.g. ZnSe, GaAs, Ge, the band gaps have contributions from: (a) a homopolar band gap, E_h, as in pure Ge, and (b) a charge transfer, C, between A and B, termed the 'ionic energy'. These are related by

$$E_g^2 = E_h^2 + C^2 \tag{2.34}$$

E_g and E_h are measured from the spectra and hence C can be calculated. C is related to the energy required for electron charge transfer in a polar bond and hence is a measure of electronegativity, as defined by Pauling. A scale of ionicity was devised:

$$\text{Ionicity}, f_i = \frac{C^2}{E_g^2} \tag{2.35}$$

Values of f_i range from zero ($C = 0$ in a homopolar covalent bond) to one ($C = E_g$ in an ionic bond) and give a measure of the fractional ionic character of a bond. Phillips analysed the spectroscopic data for 68 AB compounds with either octahedral or tetrahedral structures and found that the compounds fall into two groups separated by a critical ionicity, f_i, of 0.785.

The link between Mooser–Pearson plots and Phillips–Van Vechten ionicities is:

$$\Delta x(\text{Mooser–Pearson}) \simeq C(\text{Phillips})$$

and

$$\bar{n}(\text{Mooser–Pearson}) \simeq E_h(\text{Phillips})$$

The explanation of the latter is that as $\bar{n}$ increases, the outer orbitals become larger and more diffuse and the energy differences between outer orbitals (*s*, *p*, *d* and/or *f*) decrease; the band gap, E_h, decreases until metallic behaviour occurs at $E_h = 0$. Use of $\bar{n}$ gives the average behaviour of anion and cation. The Phillips–Van Vechten analysis has so far been restricted to AB compounds but this has provided a theoretical justification for the more widespread use and application of the readily constructed Mooser–Pearson plots.

2.13 Bond valence and bond length

The structures of most *molecular* materials—organic and inorganic—may be described satisfactorily using valence bond theory in which single, double, triple

and occasionally partial bonds occur between atoms. It may be difficult to apply valence bond theory to *non-molecular* inorganic materials, even though the bonding in them may be predominantly covalent, in cases where insufficient bonding electrons are available for each bond to be treated as an electron pair single bond.

An empirical but very useful approach to describing partial bonds in such cases has been developed by Pauling, Brown, Shannon, Donnay and others, and involves the evaluation of *bond orders* or *bond valences* in a structure. Bond valences are defined in a similar way to electrostatic bond strengths in Pauling's electrostatic valence rule for ionic structures, Chapter 1, and represent an extension of Pauling's rule to structures that are not necessarily ionic. Bond valences are defined empirically, using information on atom oxidation states and experimental bond lengths; no reference is made, at least not initially, to the nature of the bonding, whether it be covalent, ionic or some blend of the two.

Pauling's electrostatic valence rule requires the sum of the *ebs* between an anion and its neighbouring cations to equal the formal charge on the anion, equations (2.2) and (2.3). This rule may be modified to include structures which are not necessarily ionic by replacing (a) the *ebs* by the bond valence (*bv*) and (b) the formal charge on the anion by the valence of that atom (valence being defined as the number of electrons that take part in bonding). This leads to the *valence sum rule* which relates the valence, V_i, of atom i to the bond valence, bv_{ij}, between atom i and neighbouring atom j; i.e.

$$V_i = \sum_j bv_{ij} \tag{2.36}$$

Thus, the valence of an atom must equal the sum of the *bv*s for all the bonds that it forms. For cases in which bv_{ij} is an integer, this rule becomes the familiar rule that is used for evaluating the number of bonds around an atom in molecular structures, i.e. the valence of an atom is equal to the number of bonds that it forms (counting double bonds as two bonds, etc.). In non-molecular structures, however, integral *bv*s are the exception rather than the rule.

The *ebs* in Pauling's rule is given by the ratio cation charge:cation coordination number. Thus for structures in which the cation coordination is irregular or the cation–anion bonds are not all of the same length, only an average *ebs* is obtained. One advantage of the *bv* approach is that each bond is treated as an individual and hence irregularities or distortions in coordination environments are taken into account.

For a given pair of elements, an inverse correlation between *bv* and bond length exists, as shown in Fig. 2.7 for bonds between oxygen and atoms of the second row in their group valence states, i.e. Na^{I}, Mg^{II}, Al^{III}, Si^{IV}, P^{V} and S^{VI}. While each atom and oxidation (or valence) state has its own *bv*–bond length curve, 'universal curves' such as Fig. 2.7 may be used for isoelectronic series of ions. Various analytical expressions have been used to fit curves such as Fig. 2.7, including

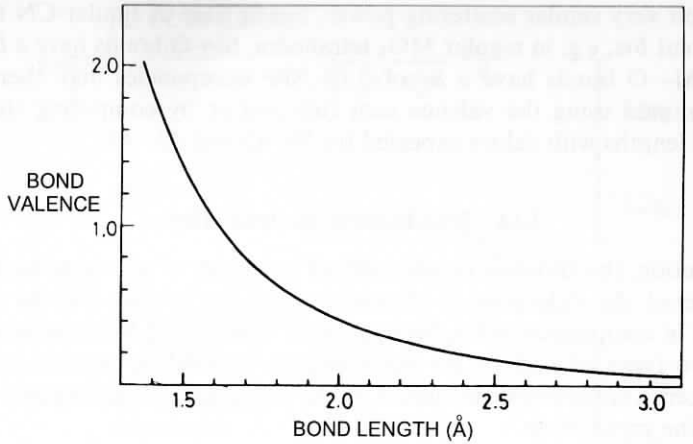

Fig. 2.7 Bond valence–bond length universal correlation curve for bonds between oxygen and second row atoms: Na, Mg, Al, Si, P and S. (From Brown, *Chem. Soc. Rev.*, 7(3), 359, 1978)

$$bv_{ij} = \left(\frac{R_0}{R}\right)^N \tag{2.37}$$

where R is the bond length and R_0, N are constant (R_0 is the value of the bond length for unit *bv*); for the elements represented by Fig. 2.7, $R_0 = 1.622$ and $N = 4.290$.

From Fig. 2.7, bond length increases with decreasing *bv*; since, for a given atom, *bv* must decrease with increasing CN, a correlation also exists between CN and bond length. This correlation was presented, in slightly different form, in Fig. 2.3, in which cation radii increase with CN. Since the data of Fig. 2.3 assume a constant radius of the fluoride or oxide ion, the ordinate in Fig. 2.3 could be changed from the ionic radius to the metal—oxygen bond length.

Curves such as Fig. 2.7 are important because they lead to an increased rationalization and understanding of crystal structures. They also have several applications that are specifically associated with structure determination, for example:

(a) As a check on the correctness of a proposed structure, since the valence sum rule should be obeyed by all atoms of the structure to within a few per cent.
(b) To locate hydrogen atoms which are often 'invisible' in X-ray structure determinations because of the very low scattering power of H. The *bv* sums around each atom are determined. If any atom shows a large discrepancy between the atom valence and the *bv*s then H is likely to be bonded to such atoms.
(c) To distinguish between Al^{3+} and Si^{4+} positions in aluminosilicate structures. By X-ray diffraction, Al^{3+} and Si^{4+} cannot be distinguished because

of their very similar scattering power, but in sites of similar CN they give different *bv*s, e.g. in regular MO_4 tetrahedra, Si—O bonds have a *bv* of one but Al—O bonds have a *bv* of 0.75. Site occupancies may therefore be determined using the valence sum rule and/or by comparing the M—O bond lengths with values expected for Si—O and Al—O.

2.14 Non-bonding electron effects

In this section, the influence on structure of two types of non-bonding electrons is considered: the *d* electrons in transition metal compounds and the s^2 pair of electrons in compounds of the heavy *p*-block elements in low oxidation states. These two types of electron do not take part in bonding as such, but nevertheless exert a considerable influence on the coordination number and environment of the metal atom.

a) *d*-electron effects

In transition metal compounds, the majority of the *d* electrons on the metal atom do not usually take part in bond formation but do influence the coordination environment of the metal atom and are responsible for properties such as magnetism. For present purposes, basic crystal field theory (CFT) is adequate to describe qualitatively the effects that occur. It is assumed that the reader is acquainted with CFT and only a summary is given here.

i) Crystal field splitting of energy levels

In an octahedral environment, the five *d* orbitals on a transition metal atom are no longer degenerate but split into two groups, the t_{2g} group of lower energy and the e_g group of higher energy, Fig. 2.8(a). If possible, electrons occupy orbitals singly, according to Hund's rule of maximum multiplicity. For d^4 to d^7 atoms or ions, two possible configurations occur, giving low spin (LS) and high spin (HS) states; these are shown for a d^7 ion in Fig. 2.9. In these, the increased energy, Δ, required to place an electron in an e_g orbital, and hence maximize the multiplicity, has to be balanced against the repulsive energy or pairing energy, *P*, which arises when two electrons occupy the same t_{2g} orbital. The magnitude of Δ depends on the ligand or anion to which the metal is bonded: for weak field anions, Δ is small and the HS configuration occurs, and vice versa for strong field ligands. Δ also depends on the metal and, in particular, to which row it belongs: generally $\Delta(5d) > \Delta(4d) > \Delta(3d)$. Consequently HS behaviour is rarely observed in the 4*d* and 5*d* series. Δ values may be determined experimentally from electronic spectra. The possible spin configurations for the different numbers of *d* electrons are given in Table 2.13.

The radii of transition metal ions depend on their *d* electron configuration, as shown in Fig. 2.10(a) for octahedrally coordinated divalent ions. With increasing atomic number, several trends occur. First, there is a gradual decrease in radius as the *d* shell is filled, as shown by the dashed line that passes through

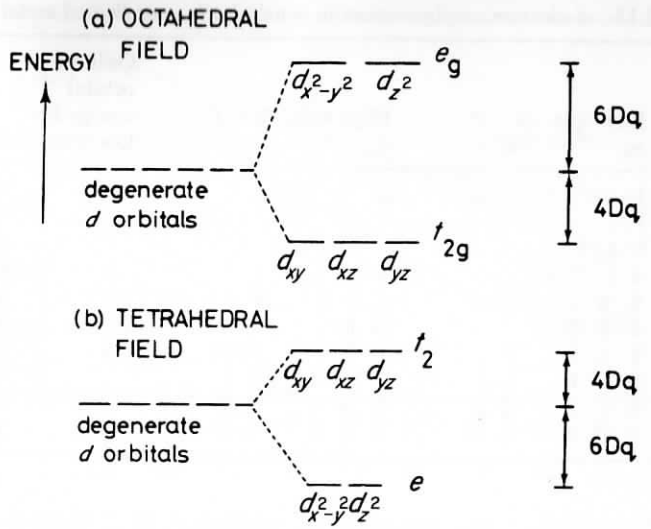

Fig. 2.8 Splitting of *d* energy levels in (a) an octahedral and (b) a tetrahedral field

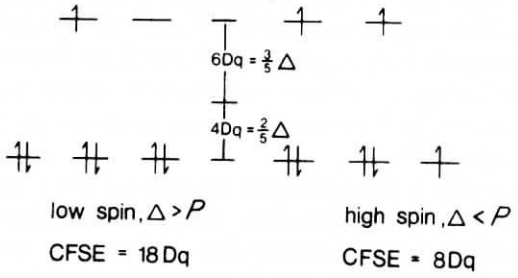

Fig. 2.9 Low and high spin states for a d^7 transition metal ion in an octahedral environment

Ca^{2+}, Mn^{2+} (HS) and Zn^{2+}. For these three ions, the distribution of *d* electron density is spherically symmetrical because the *d* orbitals are either empty (Ca), singly occupied (Mn) or doubly occupied (Zn). This decrease in radius is associated with poor shielding of the nuclear charge by the *d* electrons; hence a greater effective nuclear charge is experienced by the outer, bonding electrons resulting in a steady contraction with increasing atomic number. Similar effects occur across any horizontal row of the periodic table, but are particularly well documented for the transition metal series.

For the ions d^1 to d^4 and d^6 to d^9, the *d* electron distribution is not spherical. The shielding of the nuclear charge by these electrons is reduced even further and the radii are smaller than expected. Thus, Ti^{2+} has the configuration $(t_{2g})^2$,

Table 2.13 *d-electron configurations in octahedrally coordinated metal atoms*

Number of electrons	Low spin, $\Delta > P$ t_{2g}	e_g	High spin, $\Delta < P$ t_{2g}	e_g	Gain in orbital energy for low spin	Example
1	↑		↑			V^{4+}
2	↑ ↑		↑ ↑			Ti^{2+}, V^{3+}
3	↑ ↑ ↑		↑ ↑ ↑			V^{2+}, Cr^{3+}
4	↑↓ ↑ ↑		↑ ↑ ↑	↑	Δ	Cr^{2+}, Mn^{3+}
5	↑↓ ↑↓ ↑		↑ ↑ ↑	↑ ↑	2Δ	Mn^{2+}, Fe^{3+}
6	↑↓ ↑↓ ↑↓		↑↓ ↑ ↑	↑ ↑	2Δ	Fe^{2+}, Co^{3+}
7	↑↓ ↑↓ ↑↓	↑	↑↓ ↑↓ ↑	↑ ↑	Δ	Co^{2+}
8	↑↓ ↑↓ ↑↓	↑ ↑	↑↓ ↑↓ ↑↓	↑ ↑		Ni^{2+}
9	↑↓ ↑↓ ↑↓	↑↓ ↑	↑↓ ↑↓ ↑↓	↑↓ ↑		Cu^{2+}
10	↑↓ ↑↓ ↑↓	↑↓ ↑↓	↑↓ ↑↓ ↑↓	↑↓ ↑↓		Zn^{2+}

with two t_{2g} orbitals singly occupied. In octahedral Ti^{2+}, these non-bonding electrons occupy regions of space that are directed away from the (Ti^{2+}–anion) axes. Comparing Ti^{2+} with Ca^{2+}, for instance, Ti^{2+} has an extra nuclear charge of +2 but the two extra electrons in the t_{2g} orbitals do not shield the bonding electrons from this extra charge. Hence, Ti—O bonds in TiO are shorter than Ca—O bonds in CaO due to the stronger attraction between Ti^{2+} and the bonding electrons. This trend continues in V^{2+}, Cr^{2+} (LS), Mn^{2+} (LS) and Fe^{2+} (LS), all of which contain only t_{2g} electrons, Table 2.13. Beyond Fe^{2+} (LS), the electrons begin to occupy e_g orbitals and these do shield the nuclear charge more effectively. The radii then increase again in the series Fe^{2+} (LS), Co^{2+} (LS), Ni^{2+}, Cu^{2+} and Zn^{2+}.

For the high spin ions a different trend is observed. On passing from V^{2+} to Cr^{2+} (HS) and Mn^{2+} (HS), electrons enter the e_g orbitals, thereby shielding the nuclear charge and giving an increased radius. However, on passing from Mn^{2+} (HS) to Fe^{2+} (HS), Co^{2+} (HS) and Ni^{2+}, the additional electrons occupy t_{2g} orbitals and the radii decrease once again.

Trivalent transition metal ions show a similar trend but of reduced magnitude, Fig. 2.10(b), and the various effects that occur are effectively transferred to higher atomic number and hence to the right by one atom; thus, the smallest trivalent ion is Co^{3+} (LS) instead of Fe^{2+} (LS) which is the smallest divalent ion.

So far, only octahedral coordination of transition metal ions has been considered. Tetrahedral coordination is also common but a different energy level diagram applies to the *d* electrons. A tetrahedral field splits the *d* orbitals into two groups, but in the opposite manner to an octahedral field: three orbitals have higher energy d_{xy}, d_{xz} and d_{yz} whereas the other two, $d_{x^2-y^2}$ and d_{z^2} have lower energy, Fig. 2.8(b).

It was mentioned earlier that crystal field splitting of *d* orbitals in transition metal ions may result in *crystal field stabilization energies* (CFSE) and increased lattice energies of ionic compounds. For example, CoF_2 has the rutile structure with octahedral $Co^{2+}(d^7\text{HS})$, Fig. 2.9. The energy difference, Δ, between t_{2g}

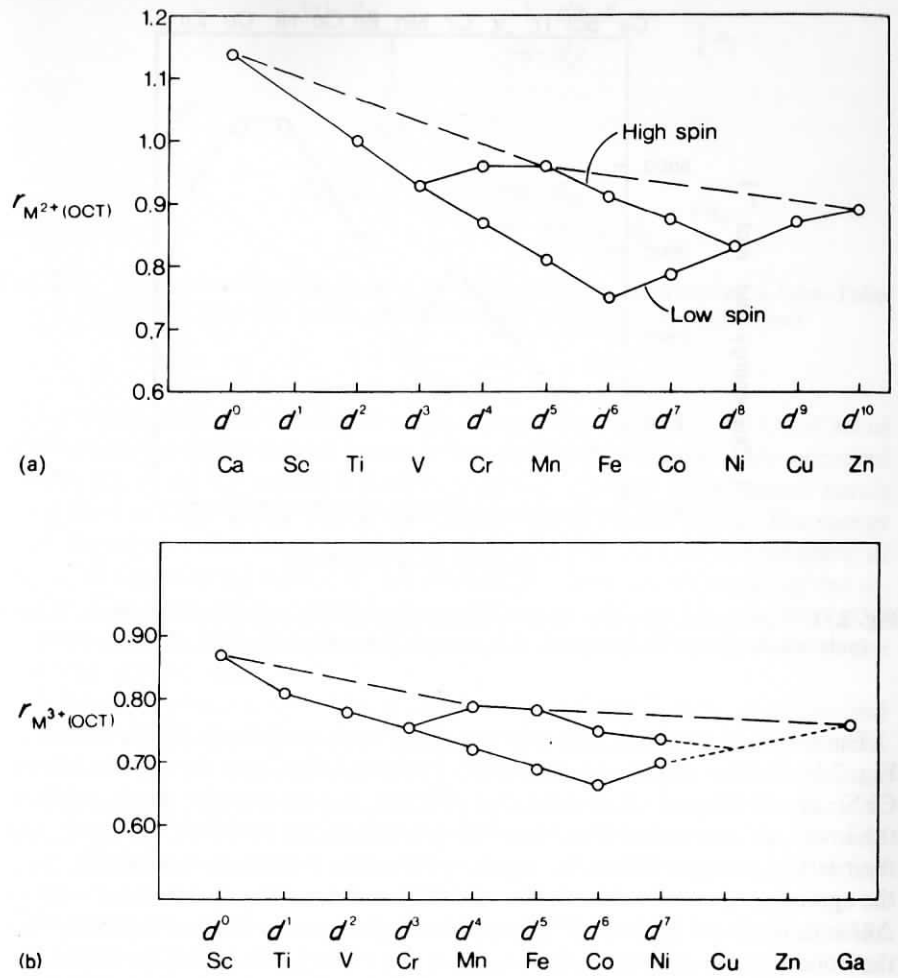

Fig. 2.10 Radii in octahedral coordination of (a) divalent and (b) trivalent transition metal ions (Shannon and Prewitt) relative to $r_{F^-} = 1.19$ Å

and e_g orbitals is set equal to 10 Dq and the t_{2g} orbitals are stabilized by an amount 4 Dq whereas the e_g orbitals are destabilized by an amount 6 Dq. Relative to five degenerate orbitals without crystal field splitting, Fig. 2.8, the CFSE of Co^{2+} in HS and LS states may be calculated. For the LS state, the CFSE is $6 \times 4\text{ Dq} - 1 \times 6\text{ Dq} = 18\text{ Dq}$. For the HS state, the CFSE is $5 \times 4\text{ Dq} - 2 \times 6\text{ Dq} = 8\text{ Dq}$.

The occurrence of CFSE leads to increased lattice energy. The CFSE calculated for Co^{2+} (HS) in rutile is 104 kJ mol^{-1}. This compares fairly well with the value of 83 kJ mol^{-1} given by the difference between the lattice energy determined from a Born–Haber cycle (2959 kJ mol^{-1}) and that calculated using the Born–Mayer equation (2876 kJ mol^{-1}).

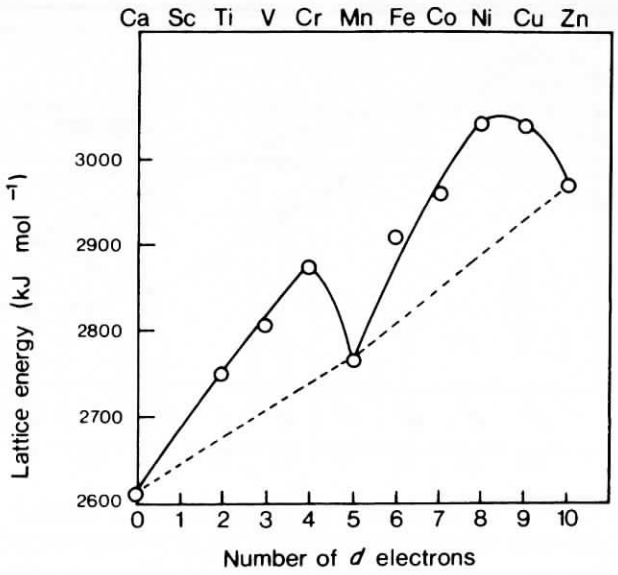

Fig. 2.11 Lattice energies of transition metal difluorides determined from Born–Haber cycle calculations. (Waddington, *Adv. Inorg. Chem. Radiochem.*, **1**, 157–221, 1959)

The lattice energies of first row transition element difluorides are shown in Fig. 2.11. Similar trends are observed for other halides. Ions that do not exhibit CFSE are d^0 (Ca), d^5 (HS) (Mn) and d^{10} (Zn), and their lattice energies fall on the lower, dashed curve. Most ions show some degree of CFSE, however, and their lattice energies fall on the upper, solid curve. For the fluorides, Fig. 2.11, the agreement between the calculated CFSE and the difference in lattice energy ΔU (i.e. U (Born–Haber) $-$ U (Born–Mayer)) is reasonable and indicates that the bonding may be treated as ionic. For the other halides, $\Delta U \gg$ CFSE and indicates that other effects, perhaps covalent bonding, must be present.

ii) Jahn–Teller distortions

In many transition metal compounds, the metal coordination is distorted octahedral and two axial bonds are either shorter than or longer than the other four bonds. The Jahn–Teller effect is responsible for these distortions in d^9, d^7 (LS) and d^4 (HS) ions. Consider the d^9 ion Cu^{2+} whose configuration is $(t_{2g})^6(e_g)^3$. One e_g orbital contains two electrons and the other contains one. The singly occupied orbital can be either d_{z^2} or $d_{x^2-y^2}$ and in a free ion situation both would have the same energy. However, since the metal ion is not a free ion but is octahedrally coordinated and the two e_g levels are occupied unequally, they are no longer degenerate. The e_g orbitals are high energy orbitals (relative to t_{2g}) since they point directly towards the surrounding ligands; electrons in the doubly occupied orbital experience stronger repulsions and have

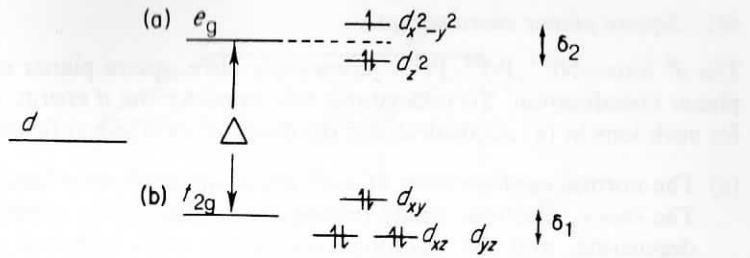

Fig. 2.12 Energy level diagram for the d-levels in a d^9 ion experiencing a Jahn–Teller distortion. The two bonds parallel to z are longer than the other four

higher energy than electrons in the singly occupied orbital. This has the effect of lengthening the metal–ligand bonds in the directions of the doubly occupied orbital, e.g. if the d_{z^2} orbital is doubly occupied, the two metal–ligand bonds along the z axis are longer than the other four metal–ligand bonds. The energy level diagram for this latter situation is shown in Fig. 2.12(a). Lengthening of the metal–ligand bond along the z axis leads to a *lowering* of energy of the d_{z^2} orbital. The distorted structure is stabilized by an amount $\frac{1}{2}\delta_2$ relative to the regular octahedral arrangement and, hence, the distorted structure becomes the observed, ground state.

High spin d^4 and low spin d^7 ions also have odd numbers of e_g electrons and show Jahn–Teller distortions. It is not clear which type of distortion is preferred (i.e. two short and four long bonds, or vice versa) and the actual shapes in a particular structure must be determined experimentally. The degeneracy of the t_{2g} levels may also be removed by the Jahn–Teller effect, but the magnitude of the splitting, δ_1 in Fig. 2.12(b), is small and the effect is relatively unimportant.

The common coordination environment of Cu^{2+} is distorted octahedral with four short and two long bonds. The distortion varies from compound to compound. In CuF_2 (distorted rutile structure), the distortion is fairly small (four F atoms at 1.93 Å, two at 2.27 Å), but is larger in $CuCl_2$ (four Cl atoms at 2.30 Å, two at 2.95 Å) and extreme in tenorite, CuO, which is effectively square planar (four O atoms at 1.95 Å, two at 2.87 Å).

The importance of Jahn–Teller distortions in Cu^{2+} and Cr^{2+} (d^4) compounds is seen by comparing the structures of the oxides and fluorides of the first-row divalent, transition metal ions. For the oxide series, MO (M^{2+} is Ti, V, Cr, Mn, Fe, Co, Ni and Cu), all have the rock salt structure with regular octahedral coordination apart from (a) CuO which contains grossly distorted (CuO_6) octahedra and possibly (b) CrO, whose structure is not known. For the fluoride series, MF_2, all have the regular rutile structure apart from CrF_2 and CuF_2 which have distorted rutile structures.

Other examples of distorted octahedral coordination due to the Jahn–Teller effect are found in compounds of Mn^{3+} (HS) and Ni^{3+} (LS).

iii) Square planar coordination

The d^8 ions—Ni^{2+}, Pd^{2+}, Pt^{2+}—commonly have square planar or rectangular planar coordination. To understand this, consider the d energy level diagram for such ions in (a) octahedral and (b) distorted octahedral fields:

(a) The normal configuration of a d^8 ion in an octahedral field is $(t_{2g})^6(e_g)^2$. The two e_g electrons singly occupy the d_{z^2} and $d_{x^2-y^2}$ orbitals, which are degenerate, and the resulting compounds, with unpaired electrons, are paramagnetic.

(b) Consider, now, the effect of distorting the octahedron and lengthening the two metal–ligand bonds along the z axis. The e_g orbitals lose their degeneracy, and the d_{z^2} orbital becomes stabilized by an amount $\frac{1}{2}\delta_2$, Fig. 2.12. For small elongations along the z axis, the pairing energy required to doubly occupy the d_{z^2} orbital is larger than the energy difference between d_{z^2} and $d_{x^2-y^2}$, i.e. $P > \delta_2$. There is no gain in stability if the d_{z^2} orbital is doubly occupied, therefore, and no reason why small distortions from octahedral coordination should be stable. With increasing elongation along the z axis, however, a stage is reached where $P < \delta_2$, and the doubly occupied d_{z^2} orbital becomes stabilized and is the preferred ground state for a d^8 ion. The distortion from octahedral coordination may be sufficiently large that the coordination becomes square planar; in many cases, e.g. PdO, there are, in fact, no axial ligands along z and, hence, the transformation from octahedral to square planar coordination is complete. Because they have no unpaired electrons, square planar compounds are diamagnetic.

Square planar coordination is more common with 4*d* and 5*d* transition elements than with 3*d* elements because the 4*d* and, especially, 5*d* orbitals are more diffuse and extend to greater radial distances from the nucleus. Consequently, the magnitude of the crystal (or ligand) field splitting (Δ, δ) caused by a particular ligand, e.g. O^{2-}, increases in the series $3d < 4d < 5d$. Thus, NiO has the rock salt structure with regular octahedral coordination of Ni^{2+} whereas PdO and PtO both have square planar coordination for the metal atoms (4*d* and 5*d*). The only known compound of Pd with octahedral Pd^{2+} is PdF_2 (rutile structure) and no octahedral Pt^{2+} or Au^{3+} compounds are known.

iv) Tetrahedral coordination

As stated earlier, a tetrahedral field splits the *d* energy levels, but in the opposite sense to an octahedral field, Fig. 2.8(b). Further, the magnitude of the splitting, Δ, is generally less in a tetrahedral field since none of the *d* orbitals point directly towards the four ligands. Rather, the d_{xy}, d_{xz} and d_{yz} orbitals are somewhat closer to the ligands than are the other two orbitals, Fig. 2.13 (only two orbital directions, d_{yz} and $d_{x^2-y^2}$ are shown). Jahn–Teller distortions again occur, especially when the upper t_2 orbitals contain 1,2,4 or 5 electrons (e.g. d^3(HS), d^4(HS), d^5 and d^9). Details are not given since various types of

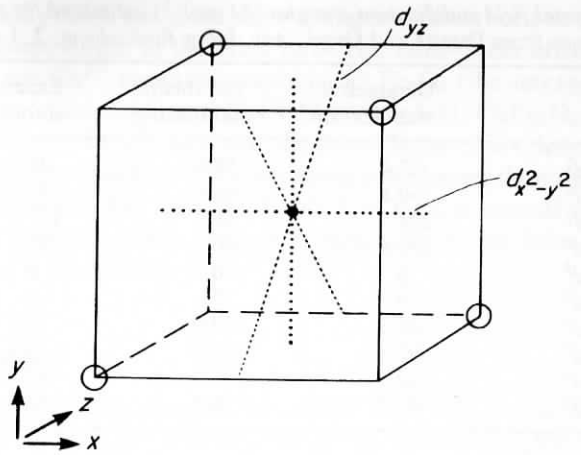

Fig. 2.13 Orientation of *d* orbitals in a tetrahedral field

distortion are possible (e.g. tetragonal or trigonal distortions) and have not been as well studied as octahedral distortions. A common type of distortion is a flattening or elongation of the tetrahedron in the direction of one of the twofold axes of the tetrahedron (e.g. along z in Fig. 2.13). An example is the flattened $CuCl_4$ tetrahedron in Cs_2CuCl_4.

v) Tetrahedral versus octahedral coordination

Most transition metal ions prefer octahedral or distorted octahedral coordination because of their large CFSE in octahedral sites. This can be estimated as follows. In octahedral coordination, each t_{2g} electron experiences a stabilization of $(4/10)\Delta^{oct}$ and each e_g electron a destabilization of $(6/10)\Delta^{oct}$. Thus Cr^{3+}, $d^3(t_{2g}^3)$ has a CFSE of $1.2\Delta^{oct}$ whereas Cu^{2+}, $d^9(t_{2g})^6(e_g)^3$, has a CFSE of $0.6\Delta^{oct}$. In tetrahedral coordination, each e electron has a stabilization of $(6/10)\Delta^{tet}$ and each t_2 electron has a destabilization of $(4/10)\Delta^{tet}$ (Fig. 2.8). Thus, Cr^{3+} would have a CFSE of $0.8\Delta^{tet}$ and Cu^{2+} would have a CFSE of $0.4\Delta^{tet}$. With the guideline that

$$\Delta^{tet} \simeq 0.4\Delta^{oct}$$

the values of Δ^{oct} and Δ^{tet} for ions may be used to predict site preferences. More accurate values may be obtained spectroscopically and are given in Table 2.14 for some transition metal oxides. High spin d^5 ions, as well as d^0 and d^{10} ions, have no particular preference for octahedral or tetrahedral sites insofar as crystal field effects are concerned. Ions such as Cr^{3+}, Ni^{2+} and Mn^{3+} show the strongest preference for octahedral coordination: thus tetrahedral coordination is rare for Ni^{2+}.

Table 2.14 *Crystal field stabilization energies (kJ mol^{-1}) estimated for transition metal oxides.* (Data from Dunitz and Orgel, *Adv. Inorg Radiochem.*, **2**, 1–60, 1960)

Ion		Octahedral stabilization	Tetrahedral stabilization	Excess octahedral stabilization
Ti^{3+}	d^1	87.4	58.5	28.9
V^{3+}	d^2	160.1	106.6	53.5
Cr^{3+}	d^3	224.5	66.9	157.6
Mn^{3+}	d^4	135.4	40.1	95.3
Fe^{3+}	d^5	0	0	0
Mn^{2+}	d^5	0	0	0
Fe^{2+}	d^6	49.7	33.0	16.7
Co^{2+}	d^7	92.8	61.9	30.9
Ni^{2+}	d^8	122.1	35.9	86.2
Cu^{2+}	d^9	90.3	26.8	63.5

The coordination preferences of ions are shown by the type of spinel structure that they adopt. Spinels have the formula AB_2O_4 (Chapter 1) and may be:

(a) normal—A tetrahedral, B octahedral;
(b) inverse—A octahedral, B tetrahedral and octahedral;
(c) some intermediate between normal and inverse.

The parameter, γ, is the fraction of A ions on octahedral sites. For normal spinel, $\gamma = 0$; for inverse, $\gamma = 1$; for a random arrangement of A and B ions, $\gamma = 0.67$. Lattice energy calculations show that, in the absence of CFSE effects, spinels of the type 2, 3 (i.e. $A = M^{2+}, B = M^{3+}$, e.g. $MgAl_2O_4$) tend to be normal whereas spinels of type 4, 2 (i.e. $A = M^{4+}, B = M^{2+}$, e.g. $TiMg_2O_4$) tend to be inverse. However, these preferences may be changed by the intervention of CFSE effects, as shown by the γ parameters of some 2, 3 spinels in Table 2.15. Examples are:

(a) All chromate spinels are normal with octahedral Cr^{3+}, consistent with the large CFSE for Cr^{3+}; ions such as Ni^{2+} are forced into tetrahedral sites in $NiCr_2O_4$.
(b) $Co_3O_4 (\equiv CoO \cdot Co_2O_3)$ is normal because low spin Co^{3+} gains more CFSE in octahedral sites than Co^{2+} loses in tetrahedral sites. Mn_3O_4 is also normal. Magnetite, Fe_3O_4, however, is inverse because whereas Fe^{3+} has no CFSE in either site, Fe^{2+} has a preference for octahedral sites.

Table 2.15 *The γ parameters of some spinels.* (Greenwood, *Ionic Crystals, Lattice Defects and Nonstoichiometry*, Butterworths, 1968; Dunitz and Orgel, *Adv. Inorg. Radiochem.*, **2**, 1, 1960)

M^{3+}	M^{2+}	Mg^{2+}	Mn^{2+}	Fe^{2+}	Co^{2+}	Ni^{2+}	Cu^{2+}	Zn^{2+}
Al^{3+}		0	0.3	0	0	0.75	0.4	0
Cr^{3+}		0	0	0	0	0	0	0
Fe^{3+}		0.9	0.2	1	1	1	1	0
Mn^{3+}		0	0	0.67	0	1	0	0
Co^{3+}		—	—	—	0	—	—	0

Spinels are usually cubic but some show tetragonal distortions in which one cell edge is of different length to the other two. The Jahn–Teller effect causes such distortions in the Cu^{2+} containing spinels, $CuFe_2O_4$ (the tetragonal unit cell parameter ratio, $c/a = 1.06$) and $CuCr_2O_4 (c/a = 0.9)$. $CuFe_2O_4$ is an inverse spinel with octahedral Cu^{2+} ions and the Jahn–Teller effect distorts the CuO_6 octahedra so that the two Cu—O bonds along z are longer than the four Cu—O bonds in the xy plane. On the other hand, $CuCr_2O_4$ is normal and the CuO_4 tetrahedra are flattened in the z direction, again due to the Jahn–Teller effect, thereby causing a shortened c axis.

b) Inert pair effect

The heavy, post-transition elements, especially Tl, Sn, Pb, Sb and Bi, commonly exhibit a valence that is two less than the group valence (e.g. the divalent state in Group IV elements, Sn and Pb). This so-called *inert pair effect* manifests itself structurally by a distortion of the metal ion coordination environment. Thus, Pb^{2+} has the configuration: (Xe core) $4f^{14}5d^{10}6s^2$, and the $6s^2$ pair is 'stereochemically active' since these electrons are not in a spherically symmetrical orbital but stick out to one side of the Pb^{2+} ion (perhaps in some kind of s–p hybridized orbital).

Various kinds of distorted polyhedra occur. Sometimes, the lone pair comes between the metal ion and some of its immediate anionic neighbours and causes a variation of bond length about the metal ion, e.g. red PbO has a structure that is a tetragonal distortion of the CsCl structure, Fig. 2.14. Four oxygens are situated at 2.3 Å from the Pb^{2+} ion, which is a reasonable Pb—O bond length, but the other four are at 4.3 Å. Although the lone pair is not directly visible, its presence is apparent from the distorted nature of the cubic coordination of Pb^{2+}.

A related effect occurs in SnS which has a distorted rock salt structure. The SnS_6 octahedra are distorted along a [111] direction such that three sulphur

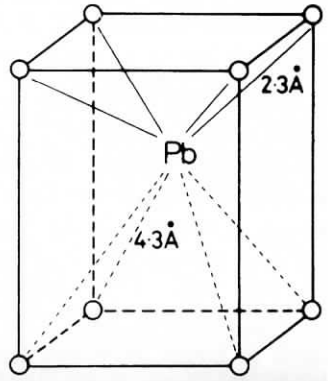

Fig. 2.14 The structure of red PbO, showing the presence of the inert pair effect by the variation in Pb—O bond distances

atoms on one side are at ~ 2.64 Å but the other three are repelled by the lone pair to a distance of ~ 3.31 Å.

Another common distortion occurs when the lone pair simply takes the place of an anion and its associated pair of bonding electrons. Five-coordinated structures result in, for example, TlI, in which one corner (anion) of the octahedron 'TlI_6' is missing.

2.15 Metallic bonding and band theory

Metallic structures and bonding are characterized by delocalized valence electrons and these are responsible for the high electrical conductivity of metals. This contrasts with ionic and covalent bonding in which the valence electrons are localized on particular atoms or ions and are not free to migrate through the structure. The bonding theory used to account for delocalized electrons is the band theory of solids. We shall not be concerned here with the mathematics of band theory but shall see qualitatively how it can be applied to certain groups of solids, especially metals and some semiconductors.

In a metal such as Al, the inner core electrons—1*s*, 2*s* and 2*p*—are localized in discrete orbitals on the individual Al atoms. However, the 3*s* and 3*p* electrons that form the valence shell occupy levels that are delocalized over the entire metal crystal. These levels are like giant molecular orbitals, each of which can contain up to two electrons. In practice, in a metal there must be an enormous number of such levels which are separated from each other by very small energy differences. Thus in a crystal of Al that contains *N* atoms, each contributes one 3*s* orbital and the result is a band of *N* closely spaced energy levels. This band is called the 3*s* *valence band*. The 3*p* levels similarly form a delocalized 3*p* band of energy levels.

The band structure of other materials may be regarded similarly. The differences between metals, semiconductors and insulators depend on:

(a) the band structure of each,
(b) whether the valence bands are full or only partly full,
(c) the magnitude of any energy gap between full and empty bands.

The band theory of solids is well supported by X-ray and photoelectron spectroscophy and by two independent theoretical approaches. The 'chemical approach' is to take molecular orbital theory, as it is usually applied to small, finite-sized molecules and extend it to infinite, 3D structures. In the molecular orbital theory of diatomic molecules, an atomic orbital from atom 1 overlaps with an atomic orbital on atom 2, resulting in the formation of two molecular orbitals that are delocalized over both atoms. One molecular orbital is 'bonding' and has lower energy than that of the atomic orbitals. The other is 'antibonding' and is of higher energy, Fig. 2.15.

Extension of this approach to larger molecules leads to an increase in the number of molecular orbitals. For each atomic orbital that is put into the system, one molecular orbital is created. As the number of molecular orbitals increases, the average energy gap between adjacent molecular orbitals must

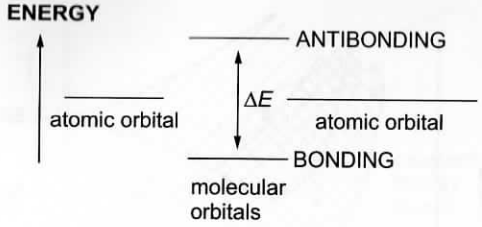

Fig. 2.15 Molecular orbitals in a diatomic molecule

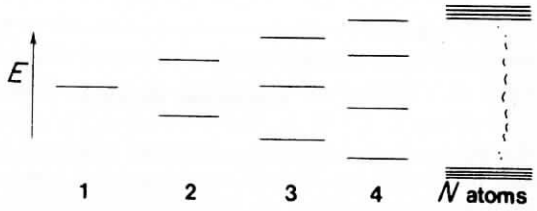

Fig. 2.16 Splitting of energy levels on molecular orbital theory

decrease, Fig. 2.16. The gap between bonding and antibonding orbitals also may decrease until essentially, a continuum of energy levels occurs.

Metals may be regarded as infinitely large 'molecules' in which an enormous number of energy levels or 'molecular' orbitals is present, ~ 6×10^{23} for one mole of metal. It is, however, no longer appropriate to refer to each level as a 'molecular' orbital since each is delocalized over all atoms in the crystal. Instead, they are usually referred to as energy levels or energy states.

The band structure of Na, calculated using the 'tight binding approximation', is shown in Fig. 2.17. The width of a particular energy band is related to the interatomic separation and hence to the degree of overlap between orbitals on adjacent atoms. Thus, at the observed interatomic separation, r_o, the 3*s* and 3*p* orbitals on adjacent atoms overlap to form broad 3*s* and 3*p* bands (shaded). The upper levels of the 3*s* band with energies in the range C to B, have similar energies to the lower levels of the 3*p* band. Hence, there is no discontinuity in energy between 3*s* and 3*p* bands. Such overlap of bands is important in explaining the metallic properties of elements such as the alkaline earths.

At the interatomic distance, r_o, the 1*s*, 2*s* and 2*p* orbitals on adjacent Na atoms do not overlap. Instead they remain as discrete atomic orbitals associated with individual atoms. They are represented in Fig. 2.17 as thin lines. If it were possible to reduce the internuclear separation from r_o to r' by compression, then the 2*s* and 2*p* orbitals would also overlap to form bands of energy levels (shaded). The 1*s* levels would, however, still be present as discrete levels at distance r'. Similar effects are likely in other elements subjected to high

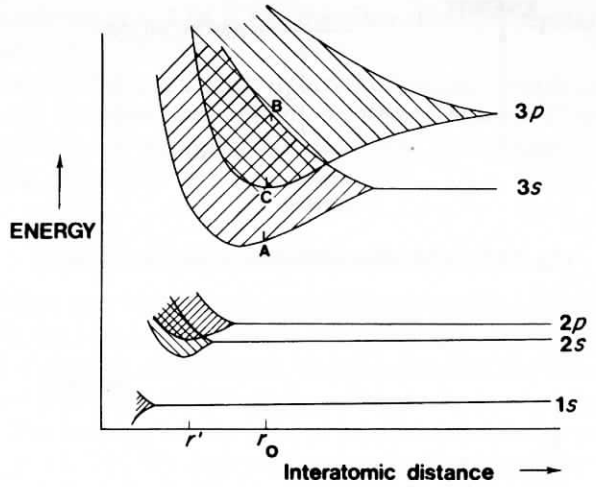

Fig. 2.17 Effect of interatomic spacing on atomic energy levels and bands for sodium, calculated using tight binding theory. Shaded areas represent bands of energy levels, formed by significant overlap of atomic orbitals on adjacent atoms

pressure. For instance, it has been calculated that hydrogen would become metallic at a pressure $\geqslant 10^6$ atm.

Sodium has the electronic configuration $1s^2 2s^2 2p^6 3s^1$ and has one valence electron per atom. Since the $3s$, $3p$ bands overlap, Fig. 2.17, the valence electrons are not confined to the $3s$ band but are distributed over the lower levels of both the $3s$ and $3p$ bands.

The 'physical approach' to band theory is to consider the energy and wavelength of electrons in a solid. In the early *free electron theory* of Sommerfeld, a metal is regarded as a potential well, inside which the more loosely held valence electrons are free to move. The energy levels that the electrons occupy are quantized (analogy with the quantum mechanical problem of a particle in a box) and the levels are filled from the bottom of the well with two electrons per level. The highest filled level at absolute zero is known as the *Fermi level*. The corresponding energy is the *Fermi energy*, E_F, Fig. 2.18. The *work function*, ϕ, is

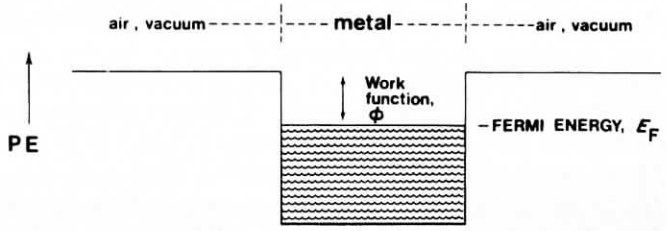

Fig. 2.18 Free electron theory of a metal; electrons in a potential well

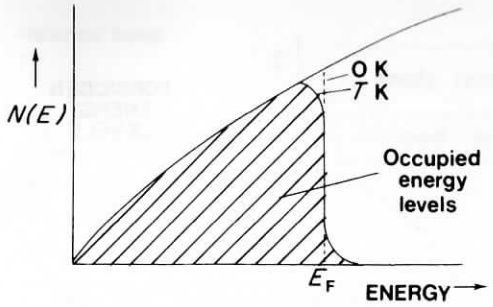

Fig. 2.19 Density of states plot on the free electron theory

the energy required to remove the uppermost valence electrons from the potential well. It is analogous to the ionization potential of an isolated atom.

A useful diagram is the *density of states, N(E)*, diagram which is a plot of the number of energy levels, $N(E)$, as a function of energy, E, Fig. 2.19. The number of available energy levels increases steadily with increasing energy in the Sommerfeld theory. Although the energy levels are quantized, there are so many and the energy difference between adjacent levels is so small that, effectively, a continuum occurs. At temperatures above absolute zero, some electrons in levels near to E_F have sufficient thermal energy to be promoted to empty levels above E_F. Hence at real temperatures, some states above E_F are occupied and others below E_F are vacant. The average occupancy of the energy levels at some temperature T above zero is shown as shading in Fig. 2.19.

The high electrical conductivity of metals is due to the drift of those electrons in half-occupied states close to E_F. Electrons in doubly occupied states lower down in the valence band cannot undergo net migration in a particular direction whereas those in singly occupied levels are free to move. The promotion of an electron from a full level below E_F to an empty one above E_F gives rise, effectively, to two mobile electrons.

The free electron theory is an oversimplification but is a very useful starting model. In more refined theories, the potential inside the crystal or well is regarded as periodic, Fig. 2.20, and not constant as in Sommerfeld's theory. The positively charged atomic nuclei are arranged in a regularly repeating manner. The potential energy of the electrons passes through a minimum at the positions of the nuclei, due to coulombic attraction, and passes through a maximum midway between adjacent nuclei. Solution of the Schrödinger equation

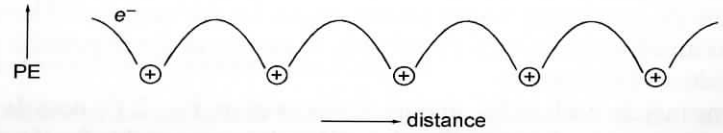

Fig. 2.20 Potential energy of electrons as a function of distance through a solid

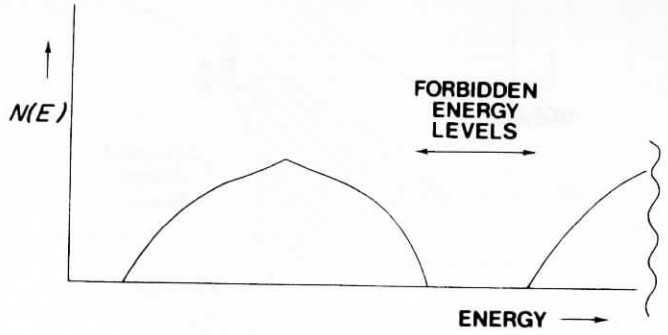

Fig. 2.21 Density of states on band theory

for a periodic potential function such as shown in Fig. 2.20 shows that an uninterrupted continuum of energy levels does not occur but, instead, only certain bands or ranges of energies are permitted for the electrons. (The forbidden energies correspond to electron wavelengths that satisfy Bragg's law for diffraction in a particular direction in the crystal.) Consequently, the density of states diagrams show discontinuities, as in Fig. 2.21.

Similar conclusions about the existence of energy bands in solids are obtained from both the molecular orbital and periodic potential approaches. From either theory, one obtains a model with bands of levels for the valence electrons. In some materials, overlap of different bands occurs. In others, a forbidden gap exists between energy bands.

Experimental evidence for the band structure of solids is obtained spectroscopically: electronic transitions between different levels may be observed. For solids, X-ray emission and absorption are useful for gaining information about both core and valence electrons. Some information about valence electrons also comes from visible and UV spectroscopy. X-ray emission spectra of solids usually contain peaks or bands of various width. Transitions between inner levels appear as sharp peaks and indicate that these levels are discrete atomic orbitals. Transitions involving valence shell electrons may give broad spectral peaks, especially for metals, indicating that valence electrons have a broad distribution of energies and are therefore located in bands.

a) Band structure of metals

In metals, the highest occupied band, the valence band, is only part full, Fig. 2.22. The occupied levels are shown schematically by the shading; some levels just below E_F are vacant whereas some above E_F are occupied. Electrons in singly occupied states close to E_F are able to move and are responsible for the high conductivity of metals.

In some metals, such as Na, energy bands overlap, Fig. 2.17: both $3s$ and $3p$ bands in Na contain electrons. Overlap of bands is responsible for the metallic properties of the alkaline earth metals as shown schematically for Be in

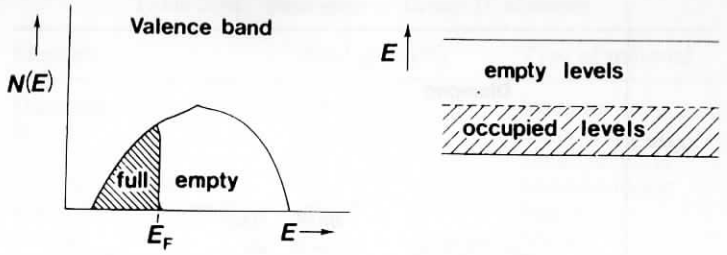

Fig. 2.22 Band structure of a metal

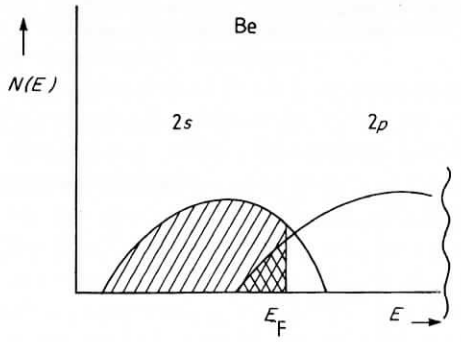

Fig. 2.23 Overlapping band structure of Be

Fig. 2.23. It has overlapping $2s$, $2p$ bands, both of which are only partly full. If the $2s$ and $2p$ bands did not overlap, then the $2s$ band would be full, the $2p$ band empty and Be would not be metallic. This is the situation that holds in insulators and semiconductors.

b) Band structure of insulators

The *valence band* in insulators is full. It is separated by a large, forbidden gap from the next energy band, which is empty, Fig. 2.24. Diamond is an excellent insulator with a band gap of ~ 6 eV. Few electrons from the valence band have sufficient thermal energy to be promoted into the empty band above. Hence the conductivity is negligibly small. The origin of the band gap in diamond is similar to that for Si, discussed next.

c) Band structure of semiconductors: silicon

Semiconductors have a similar band structure to insulators but the band gap is not very large, usually in the range 0.5 to 3.0 eV. A few electrons have sufficient thermal energy to be promoted into the empty band.

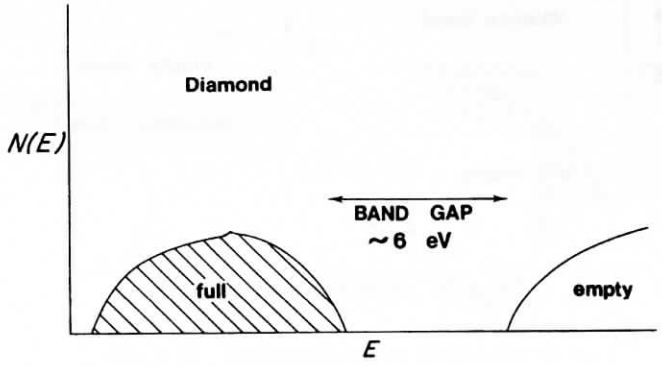

Fig. 2.24 Band structure of an insulator, carbon (diamond); the valence band is full; the conduction band is empty

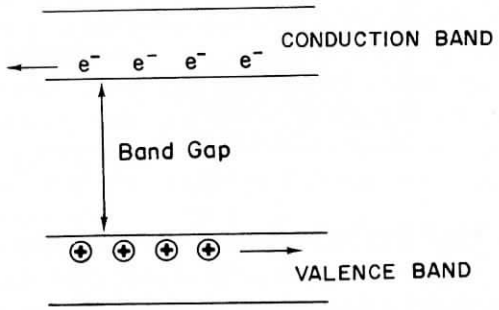

Fig. 2.25 Positive and negative charge carriers

Two types of conduction mechanism may be distinguished in semiconductors, Fig. 2.25. Any electrons that are promoted into an upper, empty band, called the *conduction band*, are regarded as negative charge carriers and would move towards a positive electrode under an applied potential. The vacant electron levels that are left behind in the valence band may be regarded as *positive holes*. Positive holes move when an electron enters them, leaving its own position vacant as a fresh positive hole. Effectively, positive holes move in the opposite direction to electrons.

Intrinsic semiconductors are pure materials whose band structure is as shown in Fig. 2.25. The number of electrons, n, in the conduction band is governed entirely by (i) the magnitude of the band gap and (ii) temperature. Pure Si is an intrinsic semiconductor. Its band gap, and that of other Group IV elements, is given in Table 2.16.

The band structure of Si is, in fact, quite different to that which might be expected by comparison with Na and Mg. In these elements, the $3s$, $3p$ levels overlap to give two broad bands, both of which are part full. If the trend

Table 2.16 *Band gaps of Group IV elements*

Element	Band gap (eV)	Type of material
Diamond, C	6.0	Insulator
Si	1.1	Semiconductor
Ge	0.7	Semiconductor
Grey Sn (>13°C)	0.1	Semiconductor
White Sn (<13°C)	0	Metal
Pb	0	Metal

continued, two similar bands would be expected in Si. The bands would be half full and Si would be metallic. Clearly this is not the case and instead Si contains two bands separated by a forbidden gap. Further, the lower band contains four electrons per Si and is full. If the forbidden gap merely corresponded to separation of s and p bands, the s band would contain only two electrons per Si. This cannot be the explanation, therefore.

Explanation of the band structure of Si lies in quantum mechanics and the fact that its crystal structure is quite different to that of Na: the structure of Na is *bcc* with a CN of eight whereas that of Si is derived from *fcc* with a CN of four. A simplified explanation of the band structure of Si (and Ge, diamond, etc.) is as follows. It starts from the observation that each Si forms four equal bonds arranged tetrahedrally; these bonds or orbitals may be regarded as sp^3 hybridized. Each hybrid orbital overlaps a similar orbital on an adjacent Si to form a pair of molecular orbitals, one bonding, σ, and the other antibonding, σ^*. Each can contain two electrons, one from each Si. The only step that remains is to allow the individual σ molecular orbitals to overlap to form a σ band; this becomes the valence band. The σ^* orbitals overlap similarly and become the conduction band. The σ band is full since it contains four electrons per Si. The σ^* band is empty.

Further discussion of semiconductors and their applications is deferred to Chapter 7.

d) Band structure of inorganic solids

So far, we have concentrated on materials that are conductors of electricity. However, many inorganic solids can also be treated profitably using band theory, whether or not they are regarded as electrical conductors. Band theory provides additional insight into the structures, bonding and properties of inorganic solids that complements that obtained with ionic/covalent models. Most inorganic materials are more complex structurally than metals and semiconducting elements. They have also received less theoretical attention of the type involving band structure calculations. Consequently, their band structures are often known only approximately.

i) III–V, II–VI and I–VII compounds

Above, we considered Group IV elements, especially Si; closely related are *III–V compounds*, such as GaP. Their valence shells are isoelectronic with

Group IV elements; they are also semiconducting. Let us now take this one stage further and consider more extreme cases, with I–VII compounds such as NaCl and II–VI compounds such as MgO.

The bonding in these is predominantly ionic. They are white, insulating solids with negligible electronic conductivity. Addition of dopants tends to produce ionic rather than electronic conductivity. On the assumption that NaCl is 100 per cent ionic, the ions have the configurations:

$$Na^+ : 1s^2 2s^2 2p^6$$
$$Cl^- : 1s^2 2s^2 2p^6 3s^2 3p^6$$

Hence, the $3s$, $3p$ valence shell of Cl^- is full and that of Na^+ is empty. Adjacent Cl^- ions are approximately in contact in NaCl and the $3p$ orbitals may overlap somewhat to form a narrow $3p$ valence band which is full. This band is composed of anion orbitals only. The $3s$, $3p$ orbitals on Na^+ ions may also overlap to form a band, the conduction band. This band is formed from cation orbitals only. It is empty under normal conditions since the band gap is large, ~ 7 eV. The band structure of NaCl is that of an insulator, Fig. 2.24, therefore, but with the additional detail that the valence band is composed of anion orbitals and the conduction band of cation orbitals. Any promotion of electrons from the valence band to the conduction band may also be regarded as back transfer of charge from Cl^- to Na^+.

This conclusion leads us to expect a correlation between the magnitude of the band gap and the difference in electronegativity between anion and cation. A large electronegativity difference favours ionic bonding. In such cases back transfer of charge from anion to cation is difficult and hence ionic solids have large band gaps. The band gaps of a variety of inorganic solids are given in Table 2.17. A quantitative relation between band gap and ionicity proposed by Phillips and van Vechten, equation (2.34) exists. The band gap is made of two components: the 'homopolar band gap' which is the band gap that

Table 2.17 *Band gaps (eV) of some inorganic solids*

I–VII compounds		II–VI compounds		III–V compounds	
LiF	11	ZnO	3.4	AlP	3.0
LiCl	9.5	ZnS	3.8	AlAs	2.3
NaF	11.5	ZnSe	2.8	AlSb	1.5
NaCl	8.5	ZnTe	2.4	GaP	2.3
NaBr	7.5	CdO	2.3	GaAs	1.4
KF	11	CdS	2.45	GaSb	0.7
KCl	8.5	CdSe	1.8	InP	1.3
KBr	7.5	CdTe	1.45	InAs	0.3
KI	5.8	PbS	0.37	InSb	0.2
		PbSe	0.27	β-SiC	2.2
		PbTe	0.33	α-SiC	3.1

Some of these values, especially for the alkali halides, are only approximate.

would be observed in the absence of any difference in electronegativity between the constituent elements and the part associated with the degree of ionic character in the bonds.

ii) Transition metal compounds

In transition metal compounds an additional important factor that influences the band structure is the presence of partly filled metal d orbitals. In some cases, these overlap to give a d band(s) and the material may have high conductivity. In other cases, d orbital overlap is limited and the orbitals are effectively localized on the individual atoms. An example of the latter is stoichiometric NiO. Its pale green colour is due to internal d–d transitions within the individual Ni^{2+} ions. It has a very low conductivity, $\sim 10^{-14}$ ohm^{-1} cm^{-1} at 25°C, and there is no evidence for significant overlap of the d orbitals to form a partly filled d band. Examples at the other extreme are TiO and VO. These have the same rock salt structure as NiO, but by contrast, d orbitals of the type d_{xy}, d_{xz}, d_{yz} on the M^{2+} ions overlap strongly, Fig. 2.26(a), to form a broad t_{2g} band. This band is only partly filled by electrons. Consequently, TiO and VO have almost metallic conductivity, $\sim 10^3$ ohm^{-1} cm^{-1} at 25°C.

An additional difference between TiO and NiO is that the t_{2g} band, capable of containing six electrons per metal atom, must be full in NiO. The two extra d electrons in Ni^{2+} are in e_g levels, d_{z^2}, $d_{x^2-y^2}$. These e_g orbitals point directly at the oxide ions, Fig. 2.26(b). Because of the intervening oxide ions, the e_g orbitals on adjacent Ni^{2+} ions cannot overlap to form a band. Hence e_g orbitals remain localized on the individual Ni^{2+} ions.

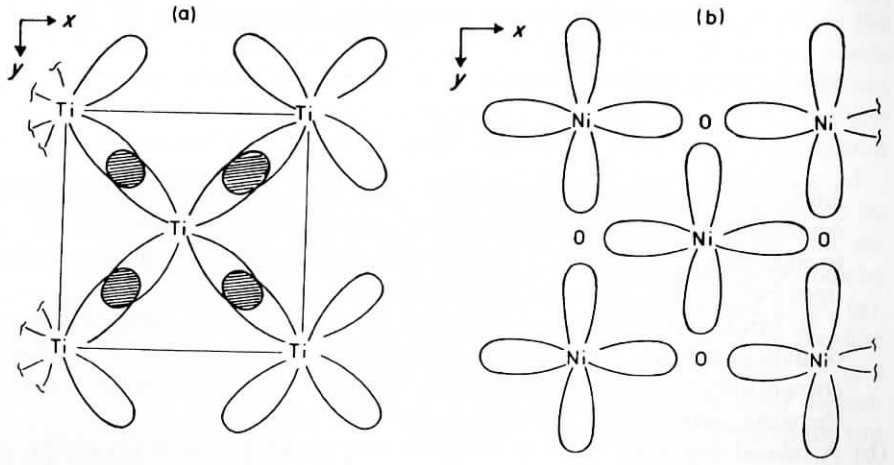

Fig. 2.26 (a) Section through the TiO structure, parallel to a unit cell face, showing Ti^{2+} positions only. Overlap of d_{xy} orbitals on adjacent Ti^{2+} ions, and similar overlap of d_{xz} and d_{yz} orbitals, leads to a t_{2g} band. (b) Structure of NiO, showing $d_{x^2-y^2}$ orbitals pointing directly at oxide ions and, therefore, unable to overlap and form an e_g band

Some guidelines as to whether good overlap of *d* orbitals is likely have been given by Phillips and Williams; *d* band formation is likely to occur if:

(a) The formal charge on the cations is small.
(b) The cation occurs early in the transition series.
(c) The cation is in the second or third transition series.
(d) The anion is reasonably electropositive.

The reasoning behind these guidelines is fairly straightforward and is based on similar arguments used in ligand field theory. Effects (a) to (c) keep the *d* orbitals spread out as far as possible and reduce the amount of positive charge that they 'feel' from their parent transition metal ion nucleus. Effect (d) is associated with reduced ionicity and band gap, as discussed earlier in this section.

A variety of examples can be found to illustrate each of the guidelines:

For (a), TiO is metallic whereas TiO_2 is an insulator. Cu_2O and MoO_2 are semiconductors whereas CuO and MoO_3 are insulators.
For (b), TiO, VO are metallic whereas NiO and CuO are poor semiconductors.
For (c), Cr_2O_3 is a poor conductor whereas lower oxides of Mo, W are good conductors.
For (d), NiO is a poor conductor whereas NiS, NiSe, NiTe are good conductors.

The *d* electron structure of solid transition metal compounds is also sensitive to the crystal structure and the oxidation state of the transition metal. Some interesting examples are provided by complex oxides with the spinel structure:

(a) Both Fe_3O_4 and Mn_3O_4 are spinels but whereas Mn_3O_4 is an insulator, Fe_3O_4 has almost metallic conductivity. The structure of Fe_3O_4 may be written as:

$$[Fe^{3+}]^{tet}[Fe^{2+}, Fe^{3+}]^{oct}O_4; \quad \text{inverse spinel}$$

whereas the structure of Mn_3O_4 is:

$$[Mn^{2+}]^{tet}[Mn_2^{3+}]^{oct}O_4; \quad \text{normal spinel}$$

Since Fe_3O_4 is inverse it contains Fe^{2+} and Fe^{3+} ions distributed over the octahedral sites. These octahedral sites are close together since they belong to edge-sharing octahedra. Consequently, positive holes can migrate easily from Fe^{2+} to Fe^{3+} ions and hence Fe_3O_4 is a good conductor.

In Mn_3O_4, the spinel is normal and the closely spaced octahedral sites contain only Mn^{3+} ions. The tetrahedral sites, containing Mn^{2+} ions, share corners only with the octahedral sites. The Mn^{2+}–Mn^{3+} distance is greater, therefore, and electron exchange cannot take place easily.

(b) A related example, which is really an example of guideline (b) above, is provided by the lithium spinels, $LiMn_2O_4$ and LiV_2O_4. Their structural formulae are similar:

$$[Li^+]^{tet}[Mn^{3+}, Mn^{4+}]^{oct}O_4$$

$$[Li^+]^{tet}[V^{3+}, V^{4+}]^{oct}O_4$$

A mixture of +3 and +4 ions is present in the octahedral sites of both but since *d* orbital overlap is greater for V than for Mn, this is reflected in the electrical properties: $LiMn_2O_4$ is a hopping semiconductor whereas LiV_2O_4 is metallic (see the sections on semiconductivity and metallic conductivity in Chapter 7 for a discussion of these properties).

iii) Fullerenes and graphite

Carbon polymorphs (or allotropes) and carbon compounds provide very good examples of how bond type can change from covalent, through semiconducting to metallic, depending on the degree of overlap of $p\pi$ orbitals on C and the extent of filling of the resulting molecular orbitals or bands. The idea of delocalization of $p\pi$ electrons stems from the unusual structure and properties of benzene, C_6H_6. Early bonding models were based on alternating single and double C–C bonds with possible resonance between two bonding configurations, Fig. 2.27(a), followed by a model with delocalization of the π electrons over all 6 C atoms in the benzene ring, (b). Overlap of *p* orbitals on adjacent C atoms is greatly assisted by the planarity of the benzene molecule, in which the p_z orbital on each C is oriented perpendicular to the plane of the molecule.

Graphite may be regarded as infinite layers of benzene molecules (c) in which the π electrons, one for each C, are delocalized over the complete layer. Band structure calculations show that the overlapping p_z orbitals give rise to two bands of levels, π and π^*, with bonding and antibonding character, as a simple extension of the π, π^* molecular orbitals in the ethene (ethylene) molecule, $CH_2{=}CH_2$ (d,e). The π, π^* levels in graphite are not discrete levels, as in C_2H_4, but form bands of levels (f). The lower π band (valence band) is full and the upper π^* band (conduction band) is essentially empty. However, the two bands do overlap by about 0.04 eV in the 3D graphite structure, which allows electrons from the valence band to be readily promoted into the conduction band. Consequently, graphite exhibits electronic conductivity (the limited amount of band overlap makes it a *semimetal*) and is a black, lustrous solid.

An interesting consequence of the band structure of graphite, linked to its layered crystal structure with a large amount of empty space in the van der Waals gap between adjacent layers, is the formation of graphite compounds by intercalation. In the formation of compounds such as C_8Na and C_8Br, (g), electrons are either added to ($C_8^-Na^+$) or withdrawn from ($C_8^+Br^-$) the graphite conduction/valence bands as part of a solid state redox reaction. Hence Na, as a reducing agent, donates electrons (h) and may be regarded as a *donor dopant*. Br by contrast is an *acceptor dopant* and creates empty electron levels at the top of the valence band (not shown).

The band structure of fullerene, C_{60}, is similar to that of graphite, but the valence and conduction bands are narrower and are separated by a band gap of 2.6 eV, Fig. 2.28. The delocalized π electron system of C_{60} is different to that of all other C-based molecular materials to date as the C_{60} molecules are not flat

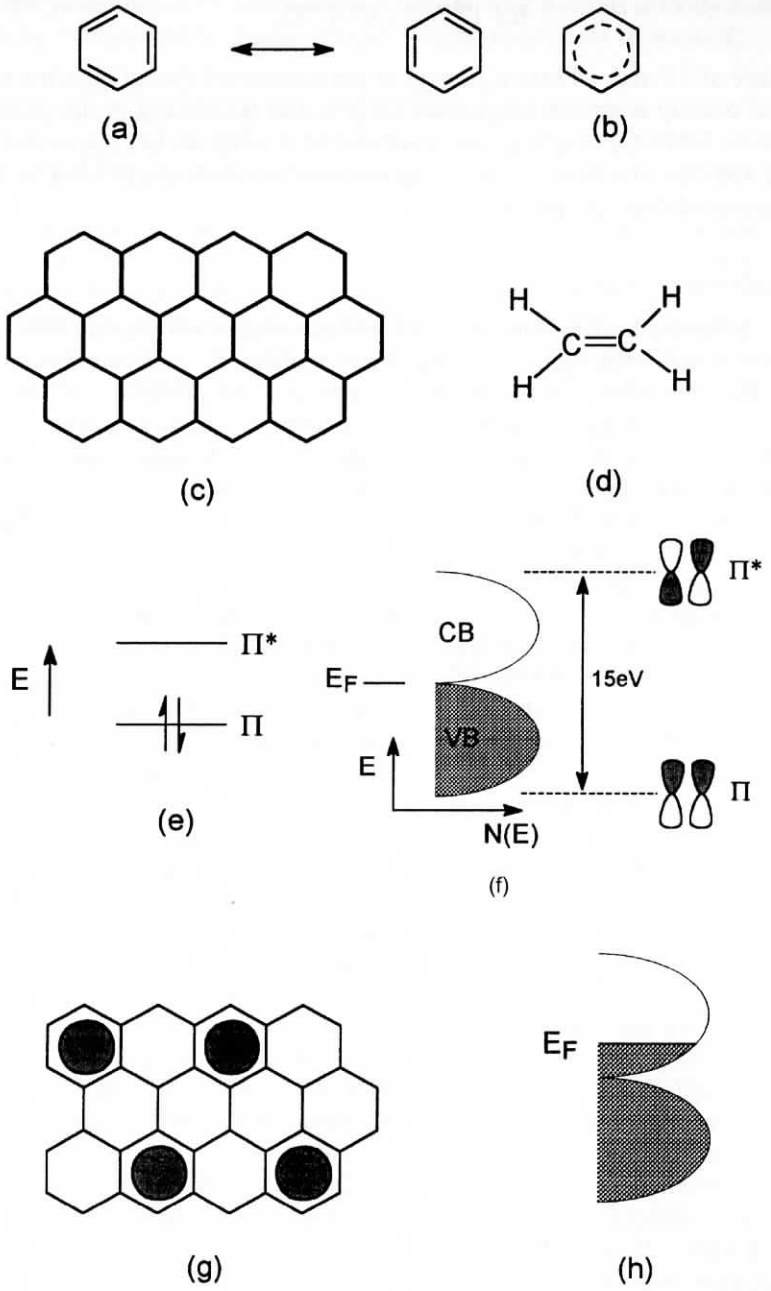

Fig. 2.27 (a) Resonating bond model to explain the structure and properties of benzene, (b) delocalized π electron model for benzene, (c) a layer of graphite, (d) the ethene molecule, (e) molecular orbitals in ethene, (f) band structure of graphite, (g) ordered arrangement of M (e.g. K, Br) between adjacent graphite layers in C_8M, and (h) band structure in C_8Na

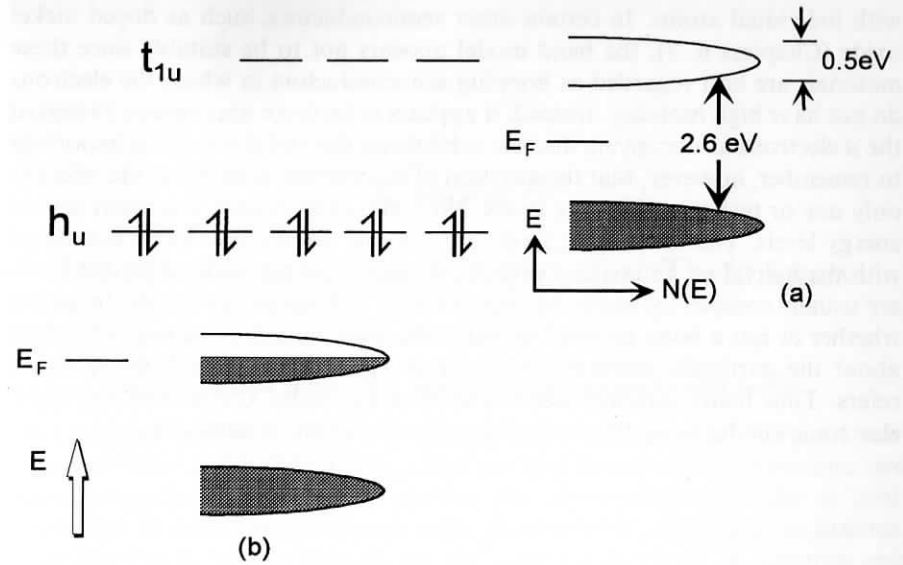

Fig. 2.28 (a) Electronic structure of C_{60} and (b) band filling in A_3C_{60}

(as in benzene, graphite, etc.), but are curved. In graphite, each 3-coordinate C is regarded as sp^2 hybridized, with bond angles of 120° and the p_z orbitals are perpendicular to the plane of the C rings. In C_{60}, the curvature of the molecule means that there is some s–p_z orbital mixing in the π orbital system. Thus, the coordination number of each C is still three, but the C atoms are above the plane of their three C neighbours rather than being coplanar with them; instead of three bond angles of 120°, as in a planar system, they are 120, 120 and 108° in C_{60}.

Electronic structure calculations show that the valence band or the 'highest occupied molecular orbitals' (HOMOs), symbol h_u, contain 10e in C_{60}. The conduction band, or the 'lowest unoccupied molecular obitals' (LUMOs), symbol t_{1u}, can contain up to 6e. C_{60} is also able to form a wide range of intercalation compounds in which C_{60} acts as an electron acceptor. Thus, in K_3C_{60} (Section 1.15f), the conduction band is half full, Fig. 2.28(b), and K_3C_{60} is metallic, in contrast to the insulating C_{60} parent.

2.16 Bands or bonds: a final comment

The three extreme types of bonding in solids are ionic, covalent and metallic. Within each category many good examples can be found. Most inorganic solids do not belong exclusively to one particular category, and then the question arises as to the most appropriate way of describing their bonding.

The band model is clearly appropriate where there are freely mobile electrons, as in metals and some semiconductors. Experimental measurements of mobility show that these electrons are highly mobile and are not associated

with individual atoms. In certain other semiconductors, such as doped nickel oxide (Chapters 6, 7), the band model appears not to be suitable since these materials are best regarded as hopping semiconductors in which the electrons do not have high mobility. Instead, it appears to be more appropriate to regard the *d* electrons as occupying discrete orbitals on the nickel ions. It is important to remember, however, that the question of conduction in nickel oxide refers to only one or two sets of energy levels. NiO, like all materials, has many sets of energy levels. The lower lying levels are full and are discrete levels associated with the individual anions and cations. At higher energy various excited levels are usually completely empty but may overlap to form energy bands. In asking whether or not a bond or band model is the most suitable, one has to be clear about the particular property or set of energy levels to which the question refers. Thus many ionically bonded solids may, under UV irradiation, show electronic conductivity that is best described in terms of band theory.

Chapter 3

Crystallography and Diffraction Techniques

3.1 General comments: molecular and non-molecular solids

The simplest and most obvious first question to ask about an inorganic substance is 'What is it?'. The methods that are used to answer this come into two main categories, depending on whether the substance is molecular or non-molecular. If the substance is molecular, whether it be solid, liquid or gaseous, identification is usually carried out by some combination of spectroscopic methods and chemical analysis. If the substance is non-molecular and crystalline, identification is usually carried out by X-ray powder diffraction supplemented, where necessary, by chemical analysis. Each crystalline solid has its own characteristic X-ray powder pattern which may be used as a 'fingerprint' for its identification. The powder patterns of most known inorganic solids are included in an updated version of the *Powder Diffraction File* (Section 3.3e); by using an appropriate search procedure, unknowns can usually be identified rapidly and unambiguously.

Once the substance has been identified, the next stage may be to determine its structure, if this is not known already. For molecular materials, details of the molecular geometry may be obtained from further spectroscopic measurements. Alternatively, if the substance is crystalline, X-ray crystallography may be used, in which case information is also obtained on the way in which the molecules pack together in the crystalline state. For molecular substances, this usually completes the story as far as identification and structure determination are concerned; attention may then focus on other matters such as properties or chemical reactivity.

For non-molecular substances, however, the word 'structure' takes on a whole new meaning. Obviously, we need to know the *crystal structure*, as given by the unit cell and its contents. However, defects and impurities are also often extremely important and sometimes control properties. Thus, the colour and lasing action of ruby, Cr-doped Al_2O_3, depend exclusively on the presence of Cr^{3+} impurities in the corundum crystal structure of Al_2O_3. In such cases, the crystal structure or *average structure* of the host is important but the *local structure* centred on the impurities or defects controls the properties.

On a somewhat larger length scale, the optical properties of colloids (or nanoparticles, to give them a name that is currently more fashionable) depend